Alginate Encapsulation of Cells to Provide a Commercially Viable Delivery for Cell Therapy

By

Maciej Kabat

A thesis submitted to the

School of Graduate Studies

Rutgers, The State University of New Jersey

In partial fulfillment of the requirements

For the degree of

Master of Science

Graduate Program in Biomedical Engineering

Written under the direction of

Martin Grumet, Ph.D.

And approved by

_____

_____

_____

New Brunswick, New Jersey

May, 2018

ABSTRACT OF THE THESIS

ALGINATE ENCAPSULATION OF CELLS TO PROVIDE A COMMERCIALLY VIABLE DELIVERY FOR CELL THERAPY

by **MACIEJ KABAT**
Thesis Director: Martin Grumet, Ph.D.

A leading cause of disease and death for all age groups are syndromes characterized by widespread uncontrollable inflammation. Severe trauma induces pro-inflammatory responses, increasing the risk of complications. Mesenchymal Stem Cells (MSCs) have the remarkable ability of altering the immune response by emitting soluble anti-inflammatory factors, which rebalance the immune system and thereby may prevent additional damage and promote recovery. Furthermore, alginate encapsulation of MSCs has proven to be an effective long-term delivery method. Encapsulation of MSCs involves a mixture of alginate and cells, which are cross-linked into microspheres with divalent cations. We hypothesized that optimization and scale-up of encapsulation of cells in alginate microspheres will provide a commercially viable solution for delivery of cell therapy.

To analyze trends and characteristics of MSC clinical trials, a novel database was constructed using data derived from ***Clinical.Trial.gov***, including data on disease targets, sources of cells, doses being delivered and routes of administration. Among the hundreds of clinical trials using free MSCs that were analyzed, several critical uncontrollable parameters may contribute to the relatively poor success rates. This includes rapid clearance in various organs, and uncertainty of numbers of surviving cells over time in target locations after transplantation. Encapsulation of MSCs in may overcome many of these challenges by prolonging MSC survival and localizing the cells in desired sites.

Alginate encapsulation involves extrusion of a mixture of cells suspended in alginate into microdroplets that crosslinked into microspheres after falling into a bath with divalent cations. We compared two modes of encapsulation, fluidic control and pressure control, holding these parameters fixed. Pressure control is advantageous over fluidic control by reducing transient and residual flow, and eliminating dead volume. Our results with pressure control show that as inner needle diameter increases flow rates increase by a power of 4. Shortening the needle increases the flow rate linearly. Thus shorter and wider needles have higher flow rates, which yield larger capsules and increased yields of encapsulated cells after a given run time using the pressure control mode. The wide dynamic range with pressure control is advantageous over the more limited fluidic control by varying needle diameters.

Measuring the number of cells per capsule is technically challenging and often not reported. The most common method for quantifying the number of live/dead cells per alginate microcapsule is imaging stained encapsulated cells using a confocal microscope. While confocal microscopy is advantageous in imaging all planes throughout a capsule, they have some disadvantages including high cost of imaging, long image acquisition time and technical limitation of measuring the number of cells per capsule in large and high density capsules. To overcome these problems, we have developed an alginate depolymerization method to visualize the contents of individual microcapsules in 2-D spreads. A key advantage of this method is that the capsules are distributed over a much larger area nearly eliminating cell overlap. This simplifies problems with confocal imaging by physically collapsing cells into a single plane rather than imaging all planes throughout the capsule and then computationally collapsing them into a single plane. In

addition, compared to confocal microscopy, measuring the viability using a epifluorescent microscope is less expensive, faster, and diminishes the cell overlapping issue because the cells are dispersed in a single plane.

TABLE OF CONTENTS

List of Figures

List of Tables

CHAPTER 1: Introduction

Mesenchymal stem/stromal cells (MSCs) are multipotent cells, which can differentiate into various different cell types including chondroblasts, adipocytes, and osteoblasts. These cells have been isolated by plastic adherence from connective tissue most commonly bone marrow, adipose, umbilical cord, and placenta [6]. MSCs are identified by their expression of characteristic patterns of markers CD29, CD73, CD90, CD105, and CD166 and their lack of CD14, CD19, CD34, CD45, and HLD-DR [1]. MSCs differentiation into mesodermal cell lines enables them to be used as a therapy for damaged tissues by engrafting them into needed areas. More importantly, they also have the ability to interact with both the innate and adaptive immune system, resulting in modulation of the immune response resulting in rapid and long lasting effects [1, 6, 7].

A leading cause of disease and death for all age groups are syndromes characterized by widespread and uncontrollable inflammation. Severe trauma induces pro-inflammatory responses, increasing the risk of tissue damage and death. Mesenchymal Stem Cells (MSCs) have remarkable abilities to alter the immune response by secreting soluble anti-inflammatory factors, which can rebalance the immune system, thereby preventing additional damage and promoting recovery [6-8]. Their primary mode of action is by secreting many anti-inflammatory cytokines and growth factors, however, they may also interact directly with pro-inflammatory macrophages, T-cells, and B-cells through cell to cell contact (Fig. 1). MSC's secreted factors have been show to modulate pro-inflammatory macrophages (M1) and promote repair by anti-inflammatory macrophages (M2), both *in vitro* and *in vivo* [1, 7].

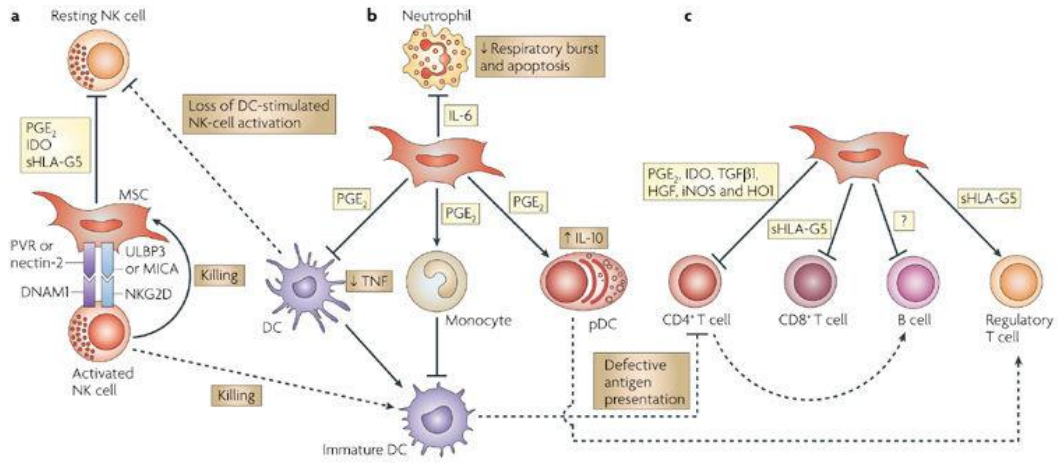

Figure. 1 shows MSC pathways for interact with both the innate and adaptive immune system through secreted factors. Adapted and modified from [1].

The therapeutic use of human MSCs has been shown in animal models for many disorders including spinal cord injury (SCI) [9], sepsis [10, 11], myocardial infarction [12], hepatic failure [13, 14], and graft versus host disease [15]. SCI has a poor prognosis due to persistent inflammation during prolonged secondary injury. Primary injury resulting from mechanical damage causes immediate cell damage and death locally. Secondary damage involves activation of pro-inflammatory M1 macrophages leading to damage in surrounding regions of the spinal cord over several weeks. Despite efficacy in using MSCs as a therapy for secondary injury in animals, there are limitations with free MSC infusion. The cells home to sites of injury but survive only transiently in vivo [16, 17]. Cell localization at the site of injury cannot be controlled [18, 19]. In addition, MSCs may differentiate into undesired cells [20]. These limitations may compromise MSC functions and slow effective clinical translation of human MSCs into therapeutics. A solution would be to immobilize MSCs in a biocompatible, semipermeable matrix while allowing MSC to secrete bioactive factors into the host.

Cell encapsulation in alginate was initially developed to treat diabetes using islets but encapsulated islets were functional in vivo for only for short periods [21]. Recent modifications yielded encapsulated islets that function for as long as 9 months in vivo [22], providing critical preclinical data for translation [23]. The polymerized alginate capsule prevents the rejection of transplanted cells by blocking attack by host immune cells. Micro-pores in the alginate capsules allow diffusion of small molecules including cytokines and nutrients while preventing higher molecular weight substances such as antibodies from entering and interacting with the cells inside [24, 25]. The high water content and pliable consistency of hydrogels make them an attractive material for cell encapsulation. Alginate is a widely used hydrogel, due to being cost effective, having mild crosslinking conditions, non-immunogenic, and FDA approved [26].

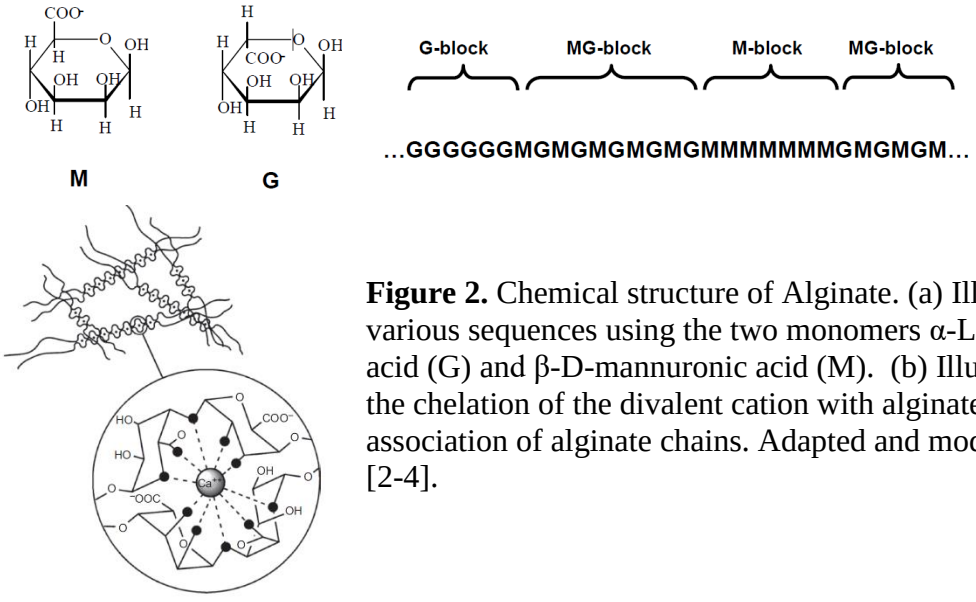

Figure 2. Chemical structure of Alginate. (a) Illustrates various sequences using the two monomers α-L-guluronic acid (G) and β-D-mannuronic acid (M). (b) Illustrates both the chelation of the divalent cation with alginate and the association of alginate chains. Adapted and modified from [2-4].

Alginate is a linear, copolymers of (1-4) glycosidic linked α-L-guluronic acid (G) and β-D-mannuronic acid (M) residue [27]. Depending on the alginate, the amount of the two monomers and their sequence in the chain can change widely (Fig. 2).

Due to the varying glycosidic linkages between the monomers, the stiffness of the molecule has been found to increase in the order MG < MM < GG [28-30].Thus, the percentage of each residue (F_G and F_M) determines the structural characteristics of the unpolymerized alginate. The wide use of alginate is due to its ability to form isotropic gels rapidly in the presence of divalent cations. The divalent cations crosslink the unpolymerized alginate into a gel. The binding affinity depends on the alginate composition and the binding strength of the ion. Studies have shown that regardless of alginate type, the order of binding strength from strongest to weakest is: Ba^{2+}, Sr^{2+}, Ca^{2+}, Mg^{2+} [27].

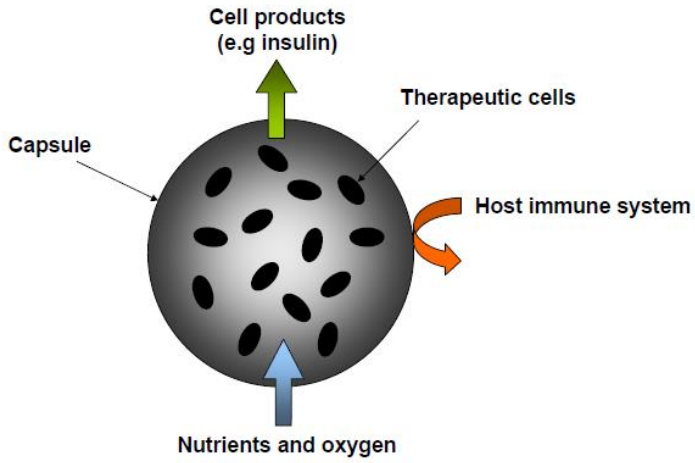

Figure 3. Encapsulated cells. Capsule consisting of cross-linked alginate are permeable to cell products and nutrients while preventing interaction with host immune system. Adapted and modified from [4].

Encapsulation involves extrusion of a mixture of unpolymerized alginate with cells from an electrostatic needle into microdroplets that are cross-linked into microspheres after falling into a bath with divalent cations. Divalent cations in the bath (e.g. $BaCl_2$) crosslink the alginate into microcapsules. Currently, commercial electrostatic cell encapsulators (e.g. NISCO, Spraybase) are available to produce uniform,

reproducible capsules. Alginate cell encapsulation has been performed with minor modifications for over 40 years. Encapsulation of MSCs in alginate is advantageous over free MSCs for several reasons (Fig. 3). Polymerized alginate prevents MSCs from migrating out of the microcapsules [31]. Encapsulation increases long-term MSC viability *in vivo*, up regulates MSC expression of many anti-inflammatory cytokines both *in vitro* [31] and *in vivo* [32], and allows the localization of MSC at sites of injection. Encapsulation prevents migration of MSC to various areas where they do not survive and thereby reduces the dose needed for efficacy [9]. In addition, encapsulated MSCs can be retrieved from the injection site to measure viability, secretory activity, and MSC differentiation at least in animal studies in which they were effective after injection in vivo in promoting functional recovery after myocardial infarction [33], hindlimb ischemia [34] and spinal cord injury [9]. In addition, genetically engineered cells secrete bioactive proteins in vivo [35-38]

There are several challenges in use of encapsulated MSCs in vivo including: 1) Host cells (e.g. macrophages) may adhere to the capsule surface, which can compromise activity and survival of the encapsulated MSC and 2) Methods to scale-up production of MSC beyond ~5 million live cells/encapsulation are not yet available. These limitations need to be resolved to facilitate the translation of encapsulated MSCs into clinical studies with enough subjects to demonstrate statistical significance. We hypothesized that optimization and scale-up of cell encapsulation in alginate microspheres will provide a commercially viable solution for delivery of cell therapy. This may be particularly relevant given our results that the number of newly registered MSC trials have been increased during the past decade but the rate of increase is plateauing, perhaps due to the

limitations using free MSCS by IV for systemic delivery. We demonstrate by using a pressure control encapsulator with an optimized needle that the encapsulation process can be scaled up to the point of clinical translation.

CHAPTER 2: Analysis of MSC Clinical Trials

2.1 Introduction:

Human MSCs have received considerable interest in clinical studies. Allogeneic MSCs have been used in clinical studies given that they induce little or no immunogenic responses. However, “free” (vs. encapsulated) MSCs survive transiently and huge doses may be needed for efficacy. There has been an increasing number of MSC clinical trials during the last decade. On 7/15/15, there were 493 total clinical trials reported using Human MSCs [39]. By 6/13/17 we found that there were 763 total clinical trials. To analyze trends and characteristics of MSC trials further, a novel database was constructed using data derived from ***Clinical.Trial.gov***, which was analyzed to include data on disease targets, sources of cells, doses being delivered and routes of administration.

2.2 Methods:

The data was extracted from *www.Clinical.Trial.gov*, as it is the largest source of registered clinical trials in the world. We searched widely for MSC or MSC-like cells that have various names. Using the term "mesenchymal" yielded the largest number of trials, which included those obtained using the search terms "mesenchymal stem cell" and "mesenchymal stromal cell." The MSC clinical trials were selected with the term "mesenchymal" on 6/13/17, which yielded 851 trials. A XML file was downloaded directly from *Clinical.Trial.gov* into Microsoft Excel, which included the **NCT number** (identifier for each trial), **title of trial**, **recruitment status**, **sponsor**, **clinical phase, country of origin** and **registration date**. We then downloaded each of the individual trial records and extracted additional information manually including the **disease**, **cell source, match, route of administration** and **dose**, which were not downloadable directly from *Clinical.Trial.gov*. However, data for all of these categories was not found in many cases. Trials that did not use MSC for therapy (e.g. mesenchymal tumors) were excluded yielding 733 trials. The analyses for each category included only those trials for which data was available, thus different numbers of trials were included for each category.

We divided clinical trials in our database into 17 groups defined by **Disease** classification. The largest group was neurological and we separated out the two largest subgroups, spinal cord injury and multiple sclerosis, accounting for more than a third of the trials. The **sources** of MSC were often found in "Interventions" but in some cases for adult bone marrow and adipose tissue it was not clear whether the source was autologous or allogenic (defined as **match**). The listing for **sponsor** in *Clinical.Trial.gov* was the

hospital, medical center, or company. We also checked each trial record to identify proprietary cells and companies sponsoring trials. Trials conducted by Athersys using Multistem were not detected with the search term "*mesenchymal.*" Based on publications describing the origin of these cells from bone marrow as Multipotent Adult Progenitor Cells (MAPCs), mesenchymal stromal cells, and bone marrow-derived mesenchymal stem cells, we have considered them as MSC-like cells and have included them in our database [40]. Combined with additional company sponsored trials that we found, the total number analyzed is 763.

Multiple **routes** of MSC administration were found and were classified into 9 groups. **Doses** in *Clinical.Trials.gov* were reported as either total numbers of cells or the numbers of cells/kg. In trials with delivery of multiple doses, for example with a dose escalation, the sum of all the cells was recorded as the dose. In trials that included different doses by different routes, we recorded all the information and used the maximal combined dose/patient for analysis. To compare doses, among trials those reported as the total number of cells were normalized to 70 kg.

2.3 Results:

The hundreds of published studies showing promising effects of MSC *in vivo,* provide a solid basis to justify the large numbers of MSC clinical trials for a wide range of conditions. Early studies show that MSCs can be as differentiated cell for replacement of lost or damaged mesenchymal tissues including cartilage or bone. MSCs are also valuable clinically because they secrete many cytokines and growth factors that modulate inflammation. However, the *Clinical.Trial.gov* registry does not include information on mechanisms of MSC treatment or the detailed characteristics of the MSCs.

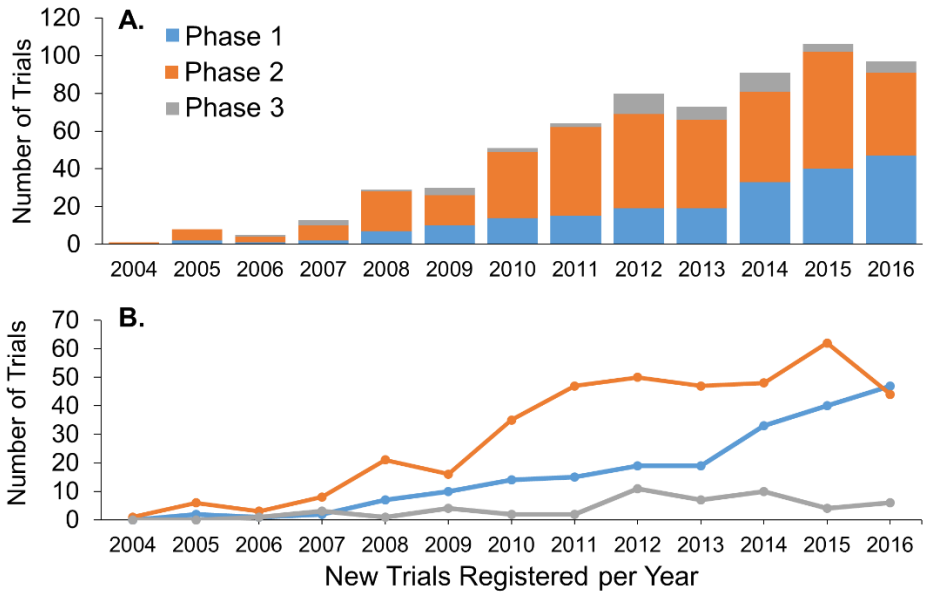

Figure 4. MSC Clinical Trials Registered at Clinical.Trial.gov (A) Total numbers of new registered clinical trials shows an increasing trend, which slows after 2012. (B).

The first use of MSCs in a clinical trial was in 2004 (Fig. 4A). The total **number** of newly registered clinical trials in each year showed an increasing trend beginning in 2008. The rate of growth slowed starting in 2014 and appeared to plateau through 2016. When the number of newly registered trials is split by **phase** as show in Fig 4B, the

number of new Phase 2 trials increased through 2011, after which the numbers appear to plateau. Due to Phase 2 trials being the most numerous, this may be the main factor responsible for the slowing trend of all new trials. By 2016, new Phase 1 trials became the major contributor. Phase 3 trials only account for 7% of all the trials. The numbers of Phase 3 trials decreased in 2014-2016 but it is a small contributor to the slowing of the total number of newly registered trials.

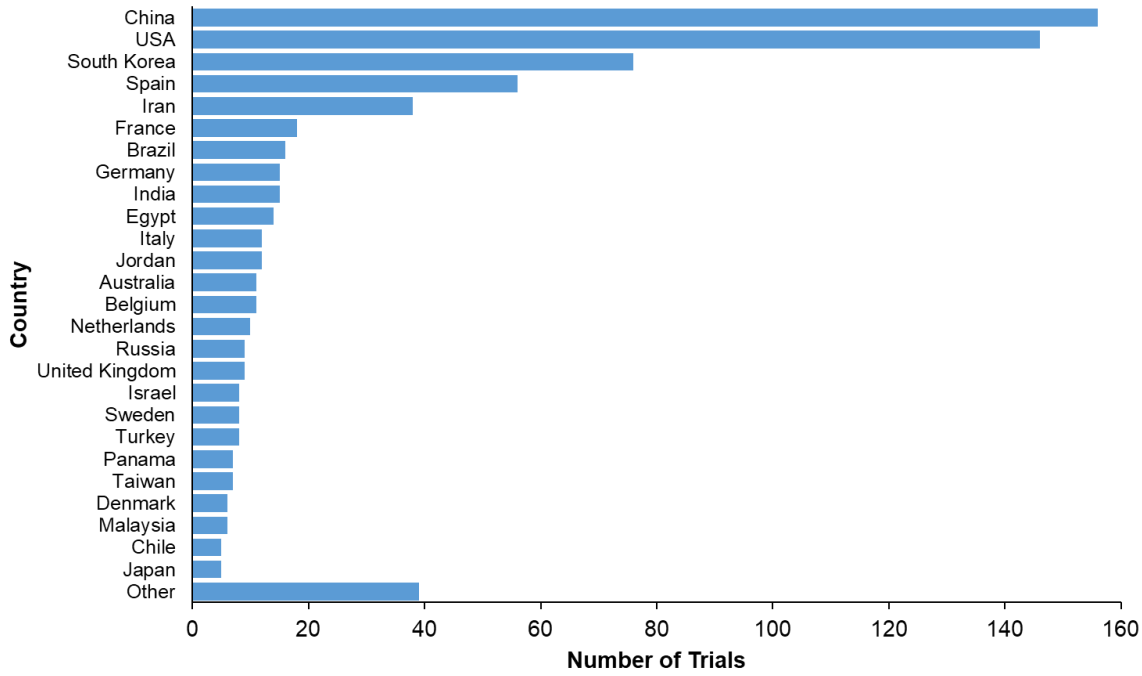

Figure 5. Total number of trials per country.

The majority of trials were conducted in China with 20% of all clinical trials followed by USA with 19% and South Korea with 10% (Fig 5). China has become a major home of clinical trials perhaps because of China's Food and Drug Administration regulations and lower costs of running clinical trials.

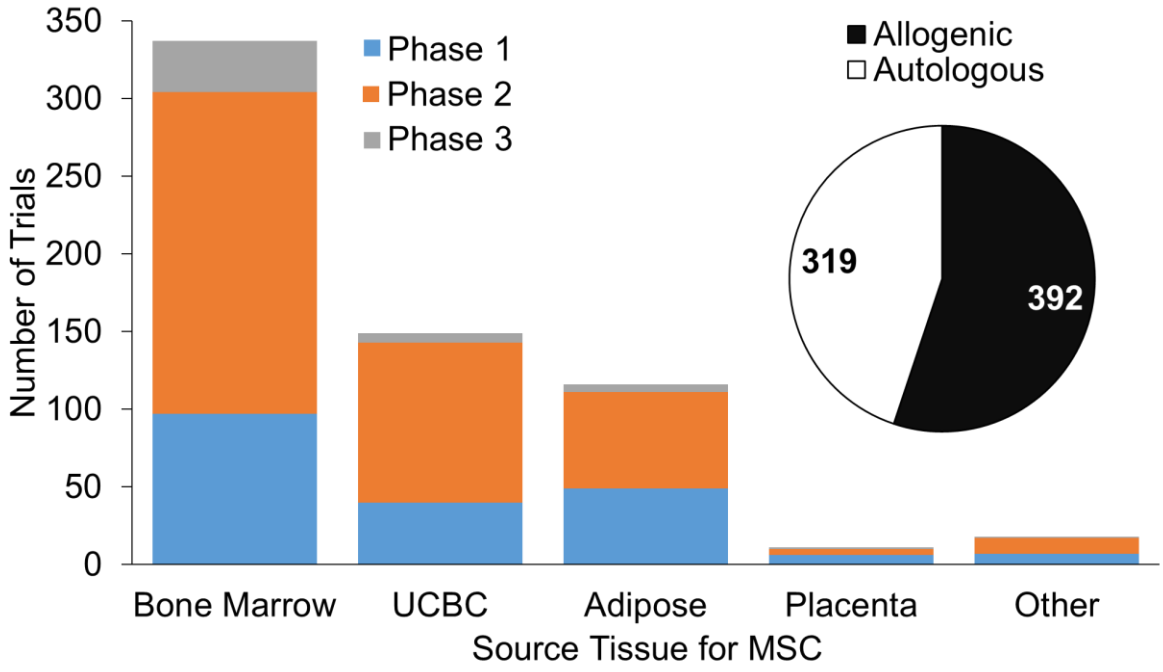

Figure 6. Number of trials using MSCs from Different Sources. Umbilical cord blood cells (UCBC) and placenta derived MSC are allogenic. Autologous MSC were derived mainly from bone marrow and adipose tissue with small numbers of other sources including dental pulp, gingiva, oral mucosa, perinatal tissue, peripheral blood, skin, menstrual blood, and stromal vascular fraction.

MSCs can be used as autologous or allogenic cell transplants, but in 8% of trials the **source** is not indicated. An autologous transplant uses the patients' own MSCs as a therapeutic treatment while an allogenic transplant uses MSCs from a different donor. About 55% of all clinical trials indicate allogenic MSCs as a therapeutic treatment (Fig. 6).

Companies are the largest source of allogenic MSCs (Fig. 7). They often isolate and produce banks of MSC-like cells for commercialization with proprietary names such as Mesenchymal precursor cells (MPC) produced by Mesoblast or Multistem produced by Athersys. These have been immuno-selected from populations of bone marrow mononuclear cells using stromal precursor antigen-1 (STRO-1), which is a marker of

early mesenchymal/stromal precursor cells associated with cell clonogenicity and plasticity [7].

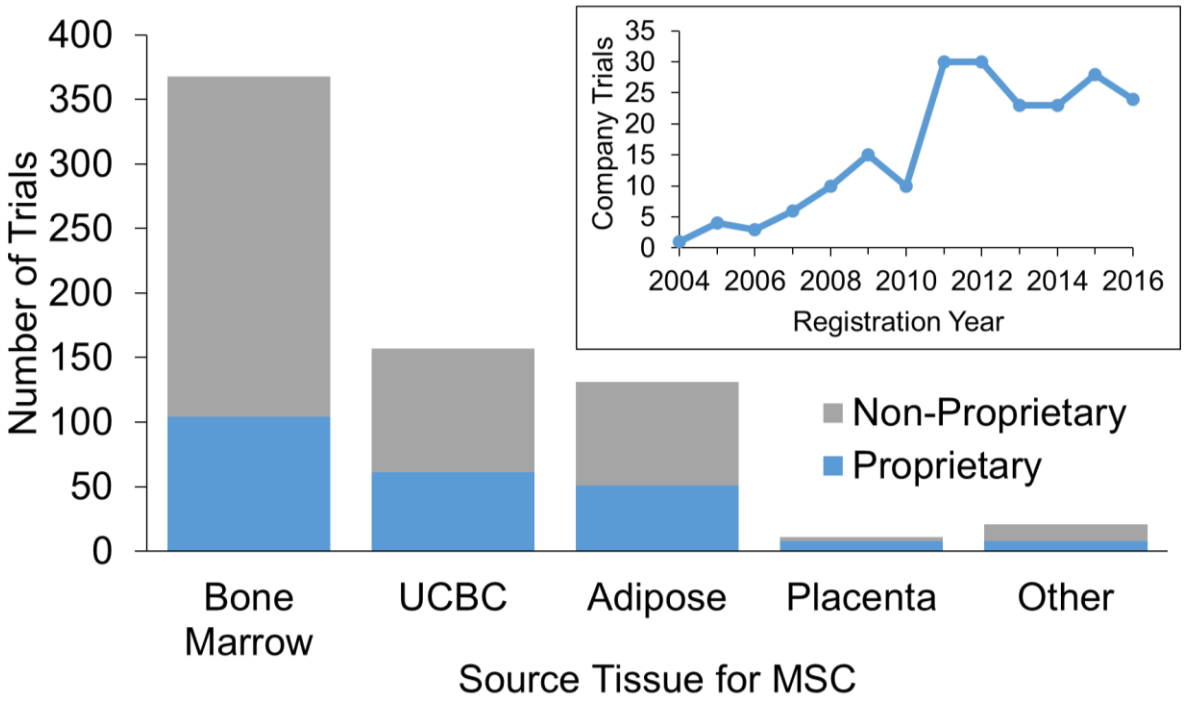

Figure 7. Clinical trials using proprietary cells or supported by a company. Proprietary trials included those sponsored by companies combined with those using proprietary MSC. Insert shows these trials, which increased though 2011 and plateaued thereafter, showing a trend similar to Phase 2 trials in Fig. 1B.

The listing for **sponsor** in *Clinical.Trial.gov* usually is the hospital or medical center. We checked each trial record to extract additional information in particular to identify proprietary cells of companies or companies sponsoring trials. All companies using proprietary cells are listed in Table 1. Over 60 companies are involved in more than 30% of clinical trials, with Mesoblast, Anterogen, and Medipost accounting for 37% of company sponsored trials. Proprietary cells were organized based on MSC source tissue in Fig. 7. The largest number of these trials use MSC from bone marrow, but the proportion of trials involving companies is higher with adipose MSC (42%) and UCBC

(38%). While only 13 trials have been registered using MSC derived from placenta, 7 of them are sponsored by Pluristem. Fig. 7 shows that the number of newly registered proprietary trials increased through 2011 and plateaued thereafter, as noted to the trend for Phase 2 trials in Fig. 4B.

Bone Marrow

Company	Trials
Mesoblast	37
Pharmicell	9
Stempeutics Research	8
Athersys	7
XCelia	7
Longeveron	4
Stemedica Cell Tech	4
Apceth	3
Celyad	3
Corestem	3
AlloCure	2
Bone Therapeutics	2
Cellonis Biotechnology	2
TCA Cellular Therapy	2
A.A. Partners	1
Brainstorm-Cell Ther	1
CardioCell	1
CellMed AG	1
Celyvir	1
HomeoTherapy	1
MD Stem Cells	1
Orbecel	1
Orthofix	1
Taiwan Bio Ther	1
Translational Biosciences	1
TOTAL	**104**

Fat

Company	Trials
Anterogen	26
Biostar Nature Cell	11
TiGenix	6
Cellular Biomedicine Group	4
CeTMAd	3
Kasiak Research	2
AlloSource	1
Cryopraxis Criobiologia	1
EHL Bio	1
EMO Biomedicine	1
Histocell	1
Nature Cell	1
Regenexx	1
Salvat Biotech	1
Steminent Biotherapeutics	1
TOTAL	**61**

Placenta

Company	Trials
Pluristem	7
CHABiotech	1
TOTAL	**8**

UCBC

Company	Trials
Medipost	20
Shenzhen Beike	7
Translational Biosciences	6
Shenzhen Hornetcorn	5
Sclnow Biotechnology	3
Kang Stem Biotech	2
Mesoblast	2
Cellonis Biotechnology	1
CHABiotech	1
CytoMed & Beike	1
Genesis Limited	1
Orbecel	1
XCelia	1
TOTAL	**51**

Other

Company	Trials
Blackstone Medical	1
Cellavita	1
Cynata Therapeutics	1
Genexine	1
Medistem	1
Rheacell	1
S-Evans Biosciences	2
TOTAL	**8**

Table 1. Companies and their number of clinical trials. Trials included those sponsored by companies combined with those using proprietary MSC.

The original **source** of MSCs was bone marrow and it is still the most frequently utilized (Fig. 6 & 7). A fraction containing MSCs can be collected from bone marrow by aspiration using needles through the pelvis. The developmentally youngest MSCs are obtained easily obtained after a birth from umbilical cord blood and placenta. Umbilical cord blood cells (UCBC) are the second most common source of MSC used for clinical trials. Adipose tissue is the third most frequent source, which most often are isolated after

liposuction. In many cases, these cells have been prepared for autologous treatment in patients. Adipose derived MSCs have also been prepared in sufficient quantities in cell banks for allogenic trials. However, many clinics and physician's offices collect fat by liposuction, partially enrich the fraction containing cells by centrifugation to remove fat and then inject the cell-enriched fraction back into the patients. In general, these are not registered and we have only included trials that have been registered in ClinicalTrial.gov. In many cases the selected cells have been rigorously characterized using the criteria outlined above for MSC. These cells are called by various names such as adipose-derived mesenchymal stem cells (AdMSC). A very small number of additional sources of MSC-like cells are from Dental Pulp, Oral Mucosa, Menstrual Blood, and Stromal Vascular Fraction, and they have been included in a category called Other.

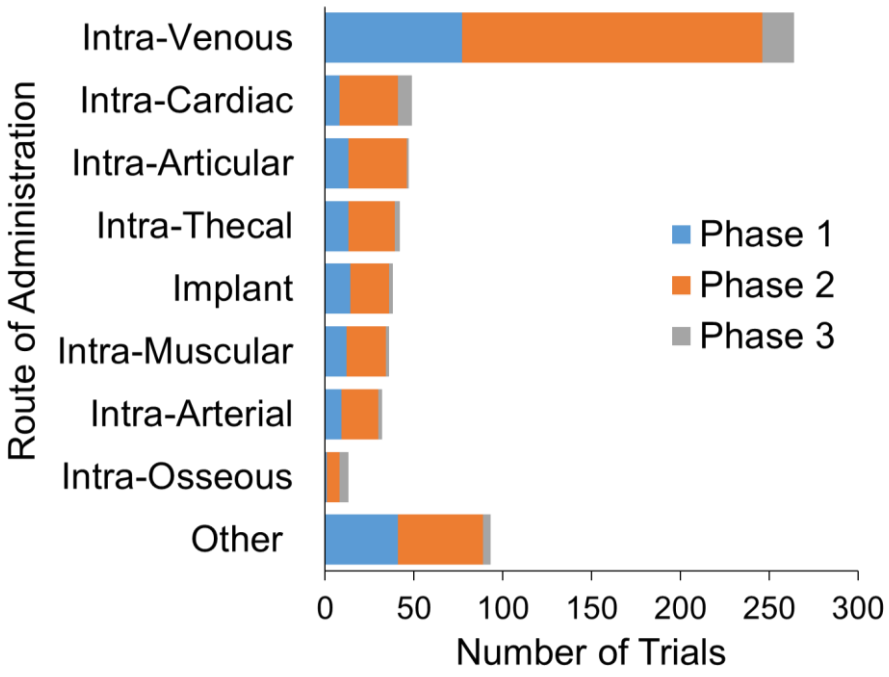

Figure 8. Routes of MSC Administration in Clinical Trials subdivided by Phases. Implant consist of MSCs embedded in biological matrices or synthetic materials.

In about 83% of the trials, we were able to extract the **routes** of delivery with the most prevalent groups shown in Fig. 8. Systemic intravenous (IV) injection is the least invasive and most common method for delivering MSCs. MSCs have also been injected directly into tissues for local treatment including Intra-Cardiac (IC), Intra-Articular (IA), Intra-Muscular (IM), Intra-osseous (IO) and Intra-thecal (IT). Implants consist of MSCs embedded in biological matrices or synthetic materials.

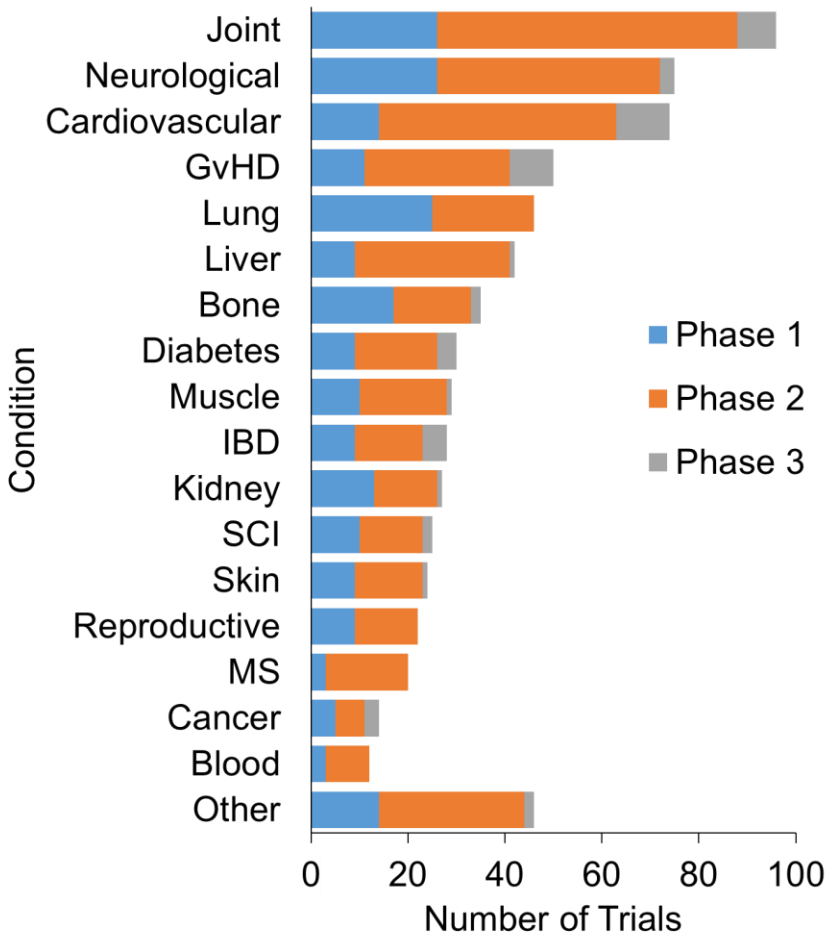

Figure 9. MSC Clinical trials by disease category subdivided by phase. 17 disease categories accounted for >90% of the trials in our database.

The type of **disease** in trials was found under the section labelled "Condition" and we classified them into the following 18 groups (Fig. 9). Joint is most common condition treated with MSCs, followed by neurological conditions, cardiovascular conditions, and Graft versus Host Disease.

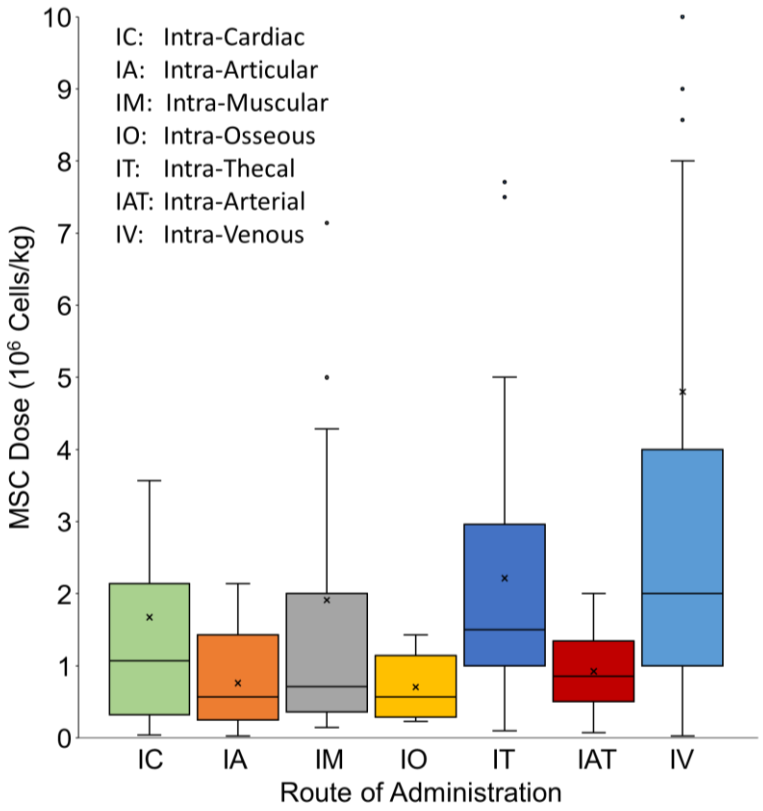

Figure 10. Analysis of dose administered in clinical trials. Box-and-Whisker Plot showing the median, average (X), quartiles and extremes (•).

The most difficult data to extract was the dose, which was possible in only ~56% of the trials. Intravenous injection, which is the most common route, used the highest MSC doses and also had the widest range (Fig. 10). Although it is the least invasive method, most MSC get trapped on first pass through the lungs [41]. Intra-Arterial injection bypasses the lungs and trials by this route used several fold lower doses in a narrower range than IV. Intra-thecal and intra-muscular doses ranged widely.

2.4 Discussion:

As the numbers of Phase 2 trials began to plateau in 2011-2013, the numbers of new Phase 3 trials increased transiently and then decreased thereafter. This may be due to limited success in the Phase 2 trials and competition for limited funding including from companies. The increasing numbers of new Phase 1 trials especially in recent years does not appear to be driving more Phase 2 trials perhaps because of lack of success. It is possible that due to the relatively lower cost of Phase 1 trials, the increase numbers of new Phase 1 trials will increase in the future. There appears to be no difference in the sources of MSCs across different phases of trials.

Many clinical trials are registered at Clinicaltrial.gov for mesenchymal stem cells (MSC) but very few have reported outcome data. Only 18% of the 763 trials reported clinically relevant results. No systematic analysis has been performed to date that analyzed dosing of free human MSCs as a clinical therapeutic. The data shown in Fig. 10 shows on average the compartmentalized route of MSCs have lower doses than the systemic routes. This may be in response to the notion that MSCs migrate away from target tissues and reduce the effective dose. Intravenous route has the widest range of doses, and Intra-Arterial has the narrowest. Intravenous delivery suffers from a pulmonary first pass effect, which sequesters most of the cells in the lungs. Intra-Arterial injection bypasses the lungs and may provide delivery of more cells to desired targets but MSCs still get trapped as they pass through other organs including the liver and spleen. Lower doses of cells are often used when they are injected directly into a tissue or compartment, for example by Intra-thecal (IT) injection to treat the spinal cord. Fig. 10

suggests a narrow effective range of dosing is being tested for certain targets of routes of administration.

Among the hundreds of clinical trials using free MSCs, several critical uncontrollable parameters may contribute to the relatively poor success rates. As shown in the above analysis, this includes rapid clearance in various organs, and uncertainty of numbers of surviving cells over time in target locations after transplantation. Encapsulation of MSCs in alginate is an innovative approach which may overcome many of these challenges. Encapsulation can decrease the cost of clinical trials by decreases the effective doses several fold lower than free MSCs in long term SCI [9]. This may be due in part to protection of MSC survival in the capsule. [5]

CHAPTER 3: Advantages of Pressure Control for Alginate Encapsulation

3.1 Introduction:

The most widely used commercial electrostatic cell encapsulator is produced by Nisco (http://www.nisco.ch). In this system, cells suspended in alginate are loaded into a syringe, which is forced by a syringe pump to extrude droplets from a needle. The droplets are driven under an electrostatic potential into a collecting vessel where they are crosslinked by divalent cations in a solution that is mixed using a stir bar. At the conclusion of the run, the apparatus is disassembled to retrieve the capsules from the collection bath for further processing. Other encapsulators from Buchi (https://www.buchi.com) and Inotech (http://www.encap.ch) are similar with more complex designs for stirring and collection but they have been used in few studies.

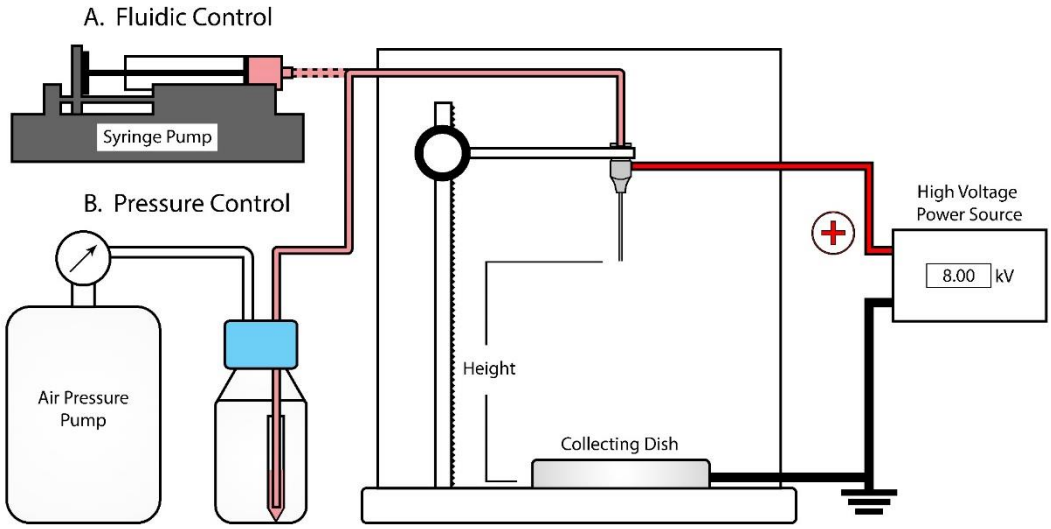

Figure 11 Spraybase encapsulator with two modes of flow controls. A) The fluidic control uses a syringe pump to drive alginate through needle. B) The pressure control uses a positive air pressure pump to drive alginate from the pressure chamber through the needle.

Spraybase (https://www.spraybase.com) is a relatively new system for encapsulation and we are not aware of any publications describing its use to encapsulate mammalian cells. It delivers the alginate solution using a pressure over fluid module and it can also operate using **peristatic** or syringe pumps similar to that used for the Nisco. Peristatic pumps produce pulsatile flows which are undesirable for cell encapsulation. Fig. 11 shows the Spraybase encapsulator using the two other modes of encapsulation: fluidic control (A) and pressure control (B). The fluidic control encapsulation mode allows for a constant flow rate between different sized needles. The pressure control encapsulation mode allows for a constant pressure between different sized needles.

The design of the Spraybase has several advantages over the Nisco. With the Nisco, any problems with elevated pressure or decreasing flow rate, for example due to a bubble in the tubing or a blockage in the needle, will terminate the run because the pressure and flow in the system cannot be reduced immediately, making changing the needle cumbersome and time-consuming. This is problematic because cell viability is compromised by increasing time in unpolymerized alginate. With the Spraybase, the pressure and flow rate can be reduced very quickly, and the needle and the tubing are easily accessible for rapid cleaning or replacement. The mixing of alginate with cells in a tube is the same in both systems, but the Nisco requires a careful transfer of the sample to the syringe avoiding formation of bubbles and has loss of sample. In contrast, the sample mixing tube is loaded directly into the Spraybase pressure chamber and the run can be started immediately by simply inserting the delivery tube without any loss of sample and time due to the transfer of the viscous mixture.

Understanding the relationship between flowrate, pressure, and needle inner radius is necessary to pick the ideal parameters for a cell encapsulation. The Hagen-Poiseuille Equation can predict this correlation:

$$Q = \frac{\pi \Delta P r_{in}^4}{8\eta l}$$

Where Q is the flow rate, ΔP is the gauge pressure, r_{in} is the inner radius of needle, η is the viscosity of alginate, and l is the length of needle.

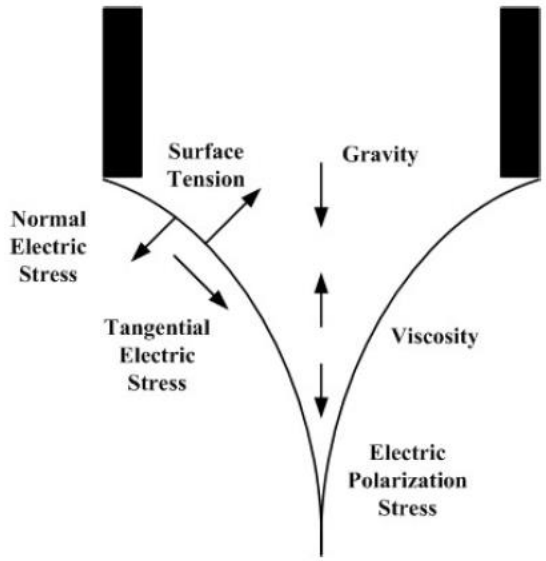

Figure 12. Distribution of forces on alginate droplets. Adapted and modified from [5].

Alginate capsules are usually limited to ~1 mm because it has been suggested that larger capsules limit perfusion of nutrients [42], which can cause cells in the center of the capsule to die. Predicting the size of capsules produced is necessary for particular applications. As shown in in Fig. 12, the major forces acting on the alginate droplet at the tip of the needle are: Surface Tension, Gravity, and Electric Force. The magnitude of the normal electric field at the tip of the stainless steel needle can be approximated by [43-45]:

$$E = \frac{\sqrt{2}\,V}{r_{out}\ln\left(\frac{4H}{r_{out}}\right)}$$

Where r_{out} is the outer radius of the needle, V is the applied voltage, H is the distance between the nozzle tip and grounded collecting dish. The force on the droplet in a non-uniform electric field is [43, 44]:

$$F_e = \frac{1}{2}\,S \cdot E^2 = 4\pi\varepsilon_0 \frac{V^2}{\ln^2\left(\frac{4H}{r_{out}}\right)}$$

Where S is the surface area of the droplet, approximated by $2\pi r_{out}^2$. Predicting the size of a capsule can be done with a modified Tate's Law. After including the force of the electric field and the droplet shrinking factor due to crosslink, the overall mass balance for a droplet formation in a non-uniform electric field can be approximated by [43]:

$$4\pi\varepsilon_0 \frac{V^2}{\ln^2\left(\frac{4H}{r_{out}}\right)} + \frac{\pi d^3}{6}\rho g = 2\pi \frac{r_{out}}{K_{SF}}\gamma\varphi$$

$$d = K_{SF} \cdot \sqrt[3]{\frac{12}{\rho g}\left(r_{out}\gamma\varphi - 2\varepsilon_0\left(\frac{V^2}{\ln^2\left(\frac{4H}{r_{out}}\right)}\right)^2\right)}$$

Where d is the capsule diameter, γ is the surface tension of alginate in air, ρ is density of alginate, K_{SF} is the shrinking factor, and φ is the Harkins correction factor. As shown in the above equation, capsule size decreases with decreasing needle outer diameter, higher voltage, and lower height.

It has been reported that flow rate and temperature can also change the size of the capsules [46, 47]. As temperature increases, surface tension and viscosity of alginate decrease, causing a decrease in capsule diameter. Increased flow rate changes the volume of alginate attached to the needle tip before the droplet detaches. As flow rate increases, the capsule diameter also increases. We used the Spraybase encapsulator to compare the pressure to fluidic modes. The bead diameter can be increased by increasing needle diameter or decreasing the applied voltage [45]. We performed a fluidic control encapsulation experiment to determine the relationship between capsule diameter and needle gauge in our system. In addition, pressure control experiments were done to determine the relationship between needle gauge and flow rate. The goal of these experiments is to develop accessible methods using commercially available instrumentation to scale-up MSC encapsulation. Experiments for this optimization were performed without cells, which allowed a wide conditions to be tested rapidly. Optimized conditions will be tested using cells, which may require additional minor optimization.

Table 2. Comparison Among Blunt 304 Stainless Steel Rame-Hart Needles

Needle Gauge	Outer Diameter (mm)	Inner Diameter (mm)	Shaft Length
21	0.813	0.508	2in
22	0.711	0.406	2in
23	0.635	0.330	1cm, 2in
24	0.559	0.305	1cm, 2in
25	0.508	0.254	1cm, 2in
26	0.457	0.254	1cm, 2in
27	0.406	0.203	1cm, 2in
28	0.356	0.178	1cm

3.2 Methods:

Alginate:

A 2.25% (w/v) sodium alginate solution was prepared by dissolving 2.25 g of PRONOVA UP LVG alginate (α-L-Guluronate/D-Mannuronate Ratio ≥ 1.5, Endotoxins ≤ 100 Eu/g) in 100 mL of DMEM Calcium Free Media (Gibco) using a hot plate with a magnetic stirrer at 45ºC. The solution was then filtered through a 0.22 µm vacuum filter. The resulting alginate had a viscosity of 330 mPa·s. The alginate solution was stored in 4ºC.

Fluidic Control of Alginate Microencapsulation using Spraybase:

The 2.25% (w/v) alginate solution was loaded into a 10 mL syringe (BD Biosciences), and attached to a syringe pump (Harvard Apparatus 22). A 1 mm inner diameter PTFE tubing (Spraybase) was attached to the syringe which was then connected to a needle (Table 2). Alginate beads were generated using an electrostatic bead generator (Spraybase) at a flow rate of 5 mL/hr, an applied voltage of 8.00 kV, using a needle height of 5 cm from the bottom of the dish at room temperature. The extruded droplets of alginate were driven electrostatically into a 50 mL collecting vessel containing 50 mM

$BaCl_2$ (Sigma-Aldrich) 145 mM NaCl, 10 mM MOPS, and 14 mM Glucose where they were polymerized for 10 min at room temperature. Microcapsules were washed with HEPES Buffer, allowed to settle under gravity and re-suspended in PBS.

Pressure Control of Alginate Microencapsulation using Spraybase:

The 2.25% (w/v) alginate solution was transferred to a 15 mL tube (Falcon Corning) and placed into to a 500 mL pressure chamber (Duran 250 mL). A 1mm diameter PTFE tubing was placed at the bottom of the alginate solution which was then connected to needle (Table 2). Alginate droplets were generated using an electrostatic bead generator (Spraybase) at a constant positive gauge pressure of 0.750 bar, an applied voltage of 8.00 kV, a needle height of 5 cm, and at room temperature. The extruded droplets of alginate were driven electrostatically into a 50 mL collecting vessel containing 50 mM $BaCl_2$ (Sigma-Aldrich), 145 mM NaCl, 10 mM MOPS, and 14 mM Glucose where they were polymerized for 10 minutes at room temperature. Spherical microcapsules were washed with HEPES Buffer, allowed to settle under gravity and were re-suspended in PBS Buffer.

Flow Rate using Needle with Different Gauges at Constant Pressure

Pressure control alginate micro-encapsulations with different configurations of needles were performed. A constant volume of 2.25% (w/v) of sodium alginate was pumped though a select needle using the protocol above. Time was started at the formation of the first droplet and stopped at the last. This time interval and the volume

were used to calculate the average flow rate of the system which was repeated 3 times per needle.

Diameter and Number of Capsules using Different Needle Gauges at Constant Flowrate

Fluidic control alginate microencapsulation with different gauge needles were performed to determine the relationship between outer needle and capsule diameters. Fluid control allows constant flow rates among various 2-inch needles. Air in the syringe will cause flow instability. Air is compressible, thus will absorb the pressure change by contracting or dilating. To keep flow rate constant throughout the run, alginate was loaded into a 10 mL syringe without air using the fluidic control protocol above. The encapsulation ran for exactly 12 minutes for 1 mL alginate, leaving excess alginate inside the tubes and syringe. Aliquots of capsules were imaged in an inverted microscope (IX81, Olympus, Tokyo, Japan) at 10x magnification and diameters for 100 capsule were measured per condition using Axiovision Program. The number of capsules were also counted to determine the total number of capsules produced.

3.3 Results:

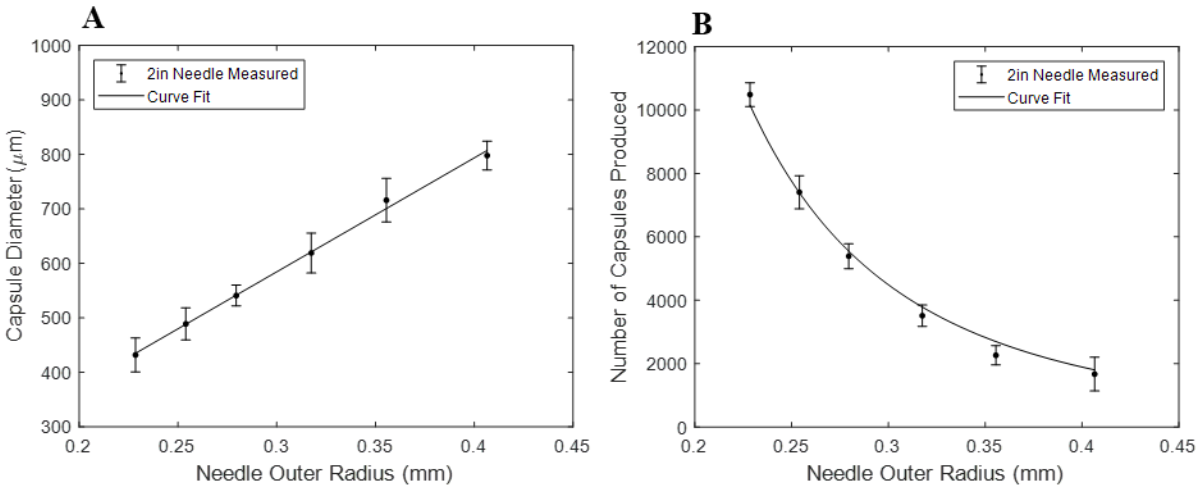

Figure 13. Capsule optimization using fluidic control encapsulator A) Capsule diameter is a linear function of needle outer radius; f(x)=2092x-43, R-squared= 0.9965. B) Number of capsules produced as a function of needle outer radius. $f(x)=(0.2021x)^{-3}$, R-squared= 0.9918

Parameters that control droplet diameter including flow rate, electric field, and needle outer diameter were also varied. The diameter of capsules was determined using the fluidic control encapsulator at 8.00 kV which allows constant flow rate and electric field strength with different needle gauges. Crosslinking in 50 mM $BaCl_2$ for 10 minutes was chosen to solidify the capsules. The diameter of alginate capsules generated using the fluidic control showed a direct relationship with outer needle diameter (Fig. 13A). As outer needle diameter increases with decreasing needle gauge, the capsule diameter increases. From 26G to 21G 2-inch needles (Table 2), capsule diameter increases from 432 ± 31 µm to 798 ± 26 µm, respectively. This is in agreement with the modified Tate's law derived above. The capsules produced with all needle gauges were highly uniform in size with less than 10% in standard deviation. The 27G 2-inch needle was not able to produce capsules at the given conditions because it vibrated, resulting in non-uniform

size and shaped capsules. This issue can be resolved by using a stronger needle or weakening the electric field.

The number of capsules produced per mL of alginate was also recorded to determine whether the shrinking factor is constant between capsule sizes. The shrinkage of hydrogels is caused by the release of water when the non-polymerized droplets make contact with the crosslinker. Determining a standard number of capsules produced per mL of alginate also allows calculation of percent alginate encapsulated. As shown in Fig. 13B, there is a strong positive correlation between the number of capsules produced and needle outer diameter. When the number of capsules produced is multiplied by the volume of a capsule, the total volume of capsules produced is constant between each needle condition, which is ~1/3 of the original un-polymerized alginate volume. This shows that the shrinking factor is constant between capsule size, as long as complete crosslinking occurs.

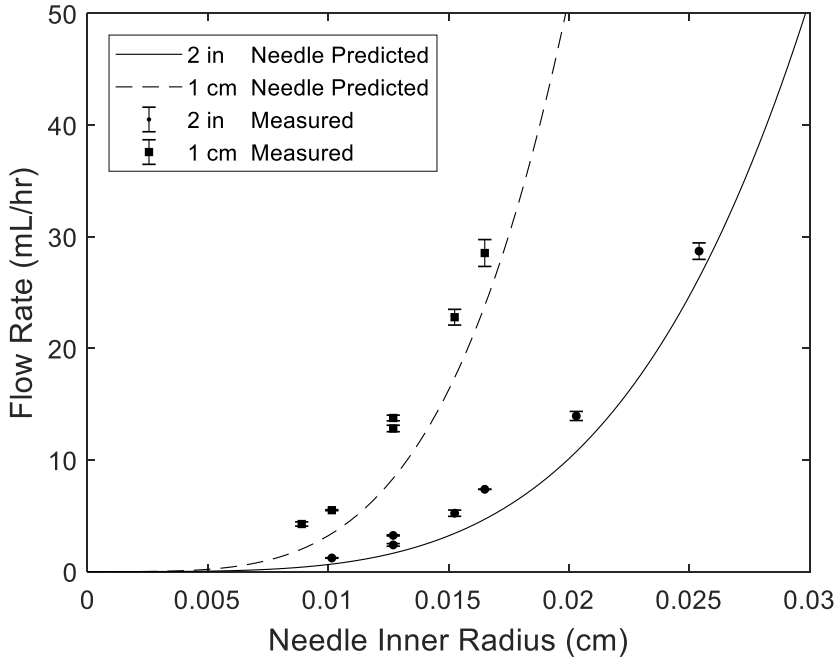

Figure 14. Flow rate as a function of needle inner radius. As predicted by the Hagen-Poiseuille Equation, as inner radius increases, flow rate increases. The viscosity of 2.25% (w/v) alginate was measured to be 330 mPa·s and used to calculate the predicted curves.

Pressure control encapsulation uses a constant positive pressure chamber to drive the flow of alginate. This yields varying flow rates for needles with different inner radii. The flow rate of different needle gauges was measured at constant positive gauge pressure of 0.750 bar, because this is the maximum pressure for consistent capsule sizes and shapes with the Spraybase system. At a constant pressure with increasing needle inner diameter, the flow rate increases by a power of 4, in agreement with the predicted values (Fig. 14). By using a 1-cm long needle instead of 2-inch, the flow rate increases by ~5X using the same gauge needles. Thus a wide range of flow rates can be selected by using needles with inner radius and controlling the pressure.

3.4 Discussion:

The electrospayer from Profector has several design features that are advantageous over the widely used Nisco. It can be set up to run, disassembled and cleaned for the next run much faster (~10 vs. ~20 minutes). It has a laser/camera imaging system to visualize the formation of a Taylor cone from the ejection nozzle and the flow in real time. Taylor cone is the electrophoretic phenomenon when the positively charged liquid at the tip of the needle deforms into a conical shape towards the more negative collecting dish. A run can be interrupted to obtain a sample for analysis. To do this, the flow is reduced and the electric field is turned off to stop formation of new droplets and a sample from the collection vessel can be obtained in <15 seconds; then the run can be restarted. It is not possible to collect a sample during a run with any other known encapsulation system including the Nisco. The sample collected can be used to determine capsule shape and size, and cell viability at the beginning of the run compared to other times during the run, which will be useful for quality control during the encapsulation process.

Pressure control encapsulations have distinct advantages over fluidic control including reduced transient flow, reduced residual flow, and zero dead volume. Transient flow occurs when pressure and flow rate vary with time during a run. Residual flow is the continuation of flow when the pump it stopped. Smaller variations occur in pressure and flow rate with the pressure than fluidic modes, which should yield a tighter capsule diameter distribution in the former. There is no sample loss with the encapsulator in the pressure mode because the delivery tubing is placed at the bottom of a conical alginate-cell mixing tube and takes up the entire sample. However, sample is lost in the transfer

from the tube to the syringe and some volume remains in the syringe at the end of a run in the fluidic system. Thus cell and capsule yield is maximized in the pressure mode. Finally, if a flow rate feedback loop is connected, the pressure control system could monitor both the flow rate and pressure.

When deciding to encapsulate using a pressure control, one should first decide what is the maximum pressure the substance can withstand, then balance needle length, needle outer-diameter, and needle inner-diameter. As inner needle diameter increases, flow rates will increase by a power of 4. Shortening the needle will increase the flow rate linearly. Shorter and wider needles have higher flow rates, which yield larger capsules.

Two ways to decrease the capsule size is by decreasing the needle outer diameter and increasing the applied voltage. Beveled needles have smaller outer diameters than their blunt counterparts, thus producing smaller capsules [9]. High electric fields do not decrease the viability of cells in microcapsules due to the Faraday cage effect. It has been reported that voltages as high as 30 kV do not decrease viability [48, 49]. The downside of using high voltages is the risk of needle vibration as we saw with the 2-inch 27G needle at 8.00 kV, 5 cm distance. Decreasing the inner needle radius should be avoided due to the lower flow rate, which has a higher risk of clogging and lower yield.

In the pressure control encapsulator, the pressure dropped moderately during a run. The Spraybase system control box does not have an automatic pressure feedback loop so the user must adjust the pressure as it changes slowly during a run. A future iteration of the system can implement a flow rate and pressure feedback loop, allowing complete independent control of encapsulation conditions.

CHAPTER 4: Depolymerizing Alginate Microcapsules to Measure Cell Viability

4.1 Introduction:

The scale-up production of encapsulated MSC in quantities suitable for clinical development of therapies (a dose of 10^7 to 10^8 cells per human) will require innovative technical methods. Most current methods are limited to yield ~ 5×10^6 live MSCs in a single preparation [9, 31, 50]. Two approaches being made by researchers to scale up encapsulated MSCs are increasing the number of capsules produced and increasing the number of cells per capsule. Nisco manufactures a 10-needle manifold which increases the production of capsules (http://www.nisco.ch/10nozzles_head.htm). However, this has a large void volume resulting in significant loss of cells and it has not been reported for use with cells. An alternative approach is to increase the density of cells per capsule. Capsules with as many as 3,000 MSCs in each 0.5-0.6 mm capsule have been created, which were stable and effective in animal studies and continued to secrete factors *ex vivo* after recovery [51].

An important technical limitation in comparing encapsulation technology among different labs is that despite many publications and reviews on the subject, critical details in measuring the number of cells per capsule is lacking, making it difficult to replicate results from different labs. The most common method for quantifying the number of live/dead cells per alginate microcapsule is imaging stained encapsulated cells using a confocal microscope. While confocal microscopy is advantageous in imaging planes throughout a capsule, they have some disadvantages. The cost of imaging is high and image acquisition time is long. When cell density exceeds ~400 cells per capsule in a 500 μm diameter capsule, overlapping of cells are not counted in the singular merged 2-D

projection image. There is no publicly available automatic cell counter for 3-D confocal images thus the number of live/dead cells can only be counted manually, e.g. ImageJ. As a result, some only report the overall percent viability instead of number of cells per capsule.

To overcome these problems, we have developed an alginate depolymerization method to visualize the contents of individual microcapsules in 2-D spreads. Because human MSC are expensive to prepare, we used rat C6 glioma cell line to prepare to optimize conditions for depolymerizing 2.25% alginate capsules because they grow rapidly and are relatively inexpensive. These cells were advantageous because they express fluorescent GFP, making it easy to observe the live cells over time. In addition, their proliferation rate is much higher than in MSCs, thus more cells can be obtained for encapsulation.

4.2 Methods:

C6 Culture:

C6 glioma cells were cultured in DMEM (Sigma Aldrich, USA) medium containing no deoxy- or ribo-nucleosides, and supplemented with 2.5% fetal bovine serum (FBS, Atlanta Biologicals, USA), 2 mM L-glutamine, and 100 U/mL penicillin. C6 cells were grown in tissue culture dishes in an incubator at 37ºC and 5% CO_2. C6 cells were allowed to proliferate to 80% confluency and collected after trypsinization with 0.5 mM EDTA. The number of cells were determined by counting in a hemocytometer [52].

Alginate Microencapsulation:

For encapsulation, trypsinized C6 cells were re-suspended in a small volume of DMEM Media with no Calcium at 10^8 cells/mL. This cell suspension was then mixed with of 2.5% (w/v) alginate (Sigma Aldrich, USA) solution to obtain a final cell density of 1×10^7 cells/mL. An electrostatic bead generator (Profector, Spraybase) was used to extrude micro-droplets from a 1 cm long 28G needle, which were subsequently cross-linked in $BaCl_2$ bath for 10 minutes as described in Chapter 3. Spherical microcapsules were washed with PBS, allowed to settle under gravity, re-suspended in cell culture medium and transferred to 25 cm^2 tissue culture flasks. This resulted in ~400 µm diameter capsule with about 500-1,000 cells per capsule.

Image Acquisition:

An aliquot of encapsulated C6 was stained with Calcein-AM and Ethidium Homodimer (Molecular Probes, USA) to determine viability. The stain was aspirated and encapsulated C6 cells were washed with phosphate buffered saline (PBS, Gibco).

Capsules were pipetted into 96 well plates, with a maximum of 10 capsules per well. The PBS was aspirated from each well, and 50mM EDTA in 1x PBS was added to each well. Capsules were allowed to depolymerize for 5 minutes. Cells settled and spread to the bottom of the well in an area ~2.5 X the diameter that of the capsules and were imaged in an inverted fluorescent microscope (IX81, Olympus, Tokyo, Japan) at 10x magnification. The tile scan option was used to stitch multiple separate images together (Zeiss AxioVision).

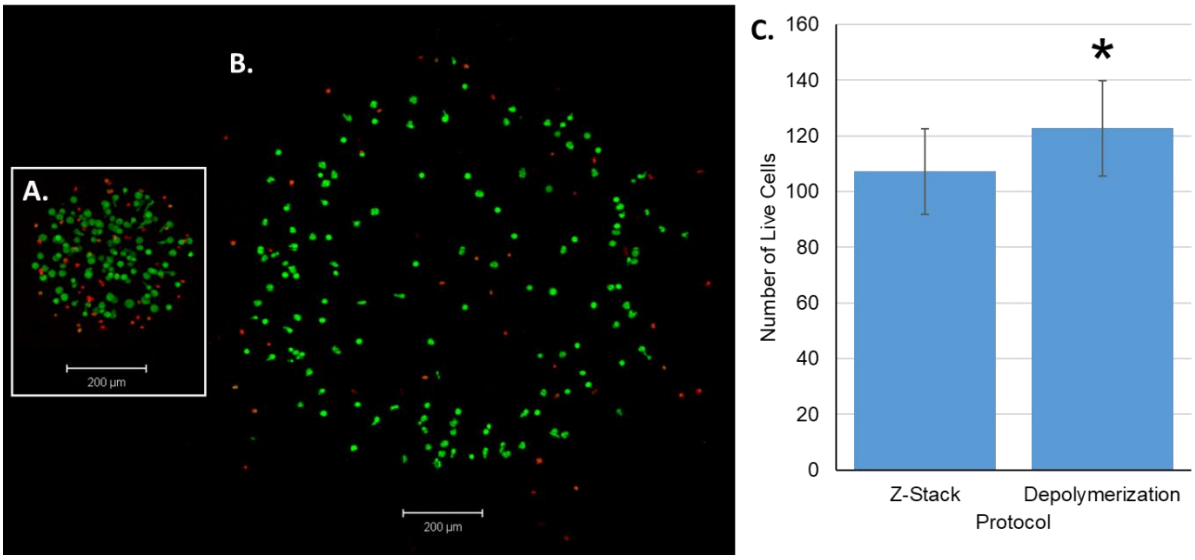

Figure 15. Depolymerization of Alginate. Data shown from the same encapsulation. A) Z-Stack image on confocal microscope of intact capsule. B) Single plane fluorescent microscope image of a depolymerized capsule. C) Number of live cells counted with the two protocols (n=15). The p-value is 0.018.

3.8 Results:

The divalent ion chelating agent Ethylenediaminetetraacetic acid (EDTA), dissociates crosslinked alginate back into its unpolymerized form. Fig. 15A shows a confocal microscope Z-stack projection of a C6 capsule. Exposure to the chelating agent causes capsules to swell ~2.5 times their original size with the cells spreading into a single plane at the bottom of a 96 well plate, which then is imaged with epifluorescence microscopy (Fig. 15B). We compared the number of live cells counted between the two protocols and found that depolymerization does not decrease the number of live cells per capsule. In fact, Fig. 15C shows significantly higher numbers of live cells were counted with the depolymerization over the confocal z-stack method. The lower number of cells counted in the z-stack protocol may be due to overlap in the confocal projections. Moreover, the spread to a much larger area that occurs in the depolymerization method reduces the overlap.

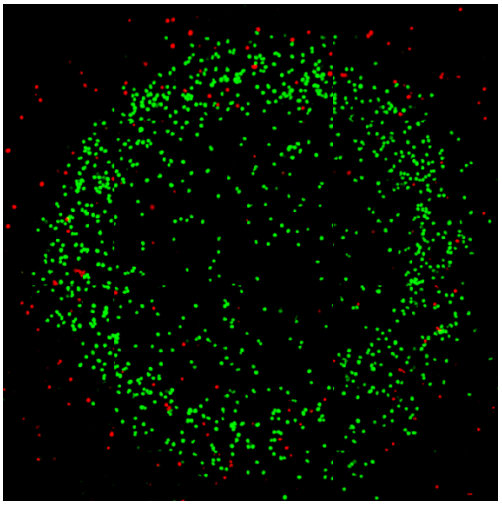

Figure 16. Depolymerized capsule imaged with a fluorescent microscope. Average 1006 live cells per capsule.

When we used the depolymerization method with high density capsules (500-1000/0.5 mm diameter capsule) we did not have an issue of cell overlap because the cells from the collapsed capsules spread over a much larger area than the cross-section of the intact capsules.

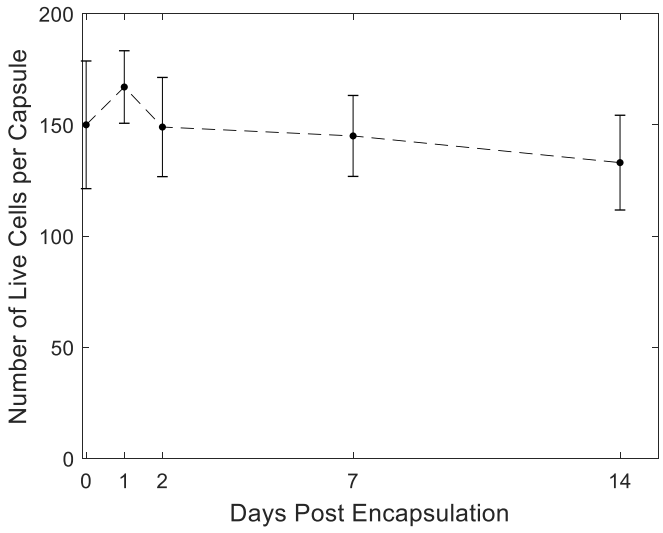

Figure 17. Number of live C6 cells per capsule over time.

This depolymerization method was used to measure the long-term viability of encapsulated C6 cells and capsules stability. As seen in Fig. 17, the number of live

encapsulated C6 cells is stable in vitro for at least to 2 weeks. Capsule morphology did not change and minimum cell division was observed with highly proliferating cells during this period.

4.4 Discussion:

This depolymerization method diminishes the technical limitation of measuring the number of cells per capsule in high density capsules. In addition, compared to confocal microscopy, measuring the viability using a epifluorescent microscope is less expensive, faster, and diminishes the cell overlapping issue because the cells are dispersed in a single plane. Although C6 cells were used instead of MSCs, these results serve a solid basis for future experiments with human MSCs. Preliminary data shows that this method also works with encapsulated Hybridomas and Chinese Hamster Ovarian cells (CHO cells) which are closer in size to the MSC than the smaller C6 cells. We designed a semi-automatic cell counter that acquires data objectively which can work for any size cell and is discussed in the Appendix. This depolymerization protocol in combination with the semi-automated cell counter can replace confocal imaging by being more sensitive, faster and less expensive.

APPENDIX: A Semi-Automated Counter for Live and Dead Cells from Depolymerized Alginate Capsules

A.1 Introduction:

The depolymerization method described in Chapter 4 diminishes technical limitations of measuring the number of cells per capsule in high density capsules. In this Appendix, we describe the development and use of an objective counting method that is particularly useful for measuring the numbers of cells/capsule. We were motivated to do this for several reasons. Publicly available automated cell counters, e.g. ImageJ, are inadequate for analyzing images resulting from depolymerization, because they lack the ability to segment individual capsules and fail with poor resolution photos [53]. Commercially available software enables users to quantify the number of cells. However, this software contains expensive proprietary algorithms which cannot be modified.

We developed an objective counter that identifies and counts fluorescent cells, whether they intrinsically express GFP or live/dead staining with green (Calcien-AM) and red fluorescence (Ethidium Homodimer), respectively. We modeled our algorithm after that of Yongming Chen, which segments individual cells using an internal and external watershed marker [53]. Watershed is a region-based segmentation technique that is able to divide groups based on the intensity of a grayscale image. We used the rat C6 glioma cells in 2.25% (w/v) alginate capsules to optimize conditions for the algorithm. In order to test the quality of our new program, the results from our automatic counter are compared to a manual human counter.

A.2 Materials and Methods:

C6 Culture, Microencapsulation, Depolymerization, & Image Acquisition

Refer to Chapter 4 methods.

Computer

A 64-bit Windows 10 Home Edition laptop with a 2.70GHz Intel i5-7200U, 8GB of RAM and 256 solid state drive was used. MATLAB R2017a was used to run the semi-automated cell counter.

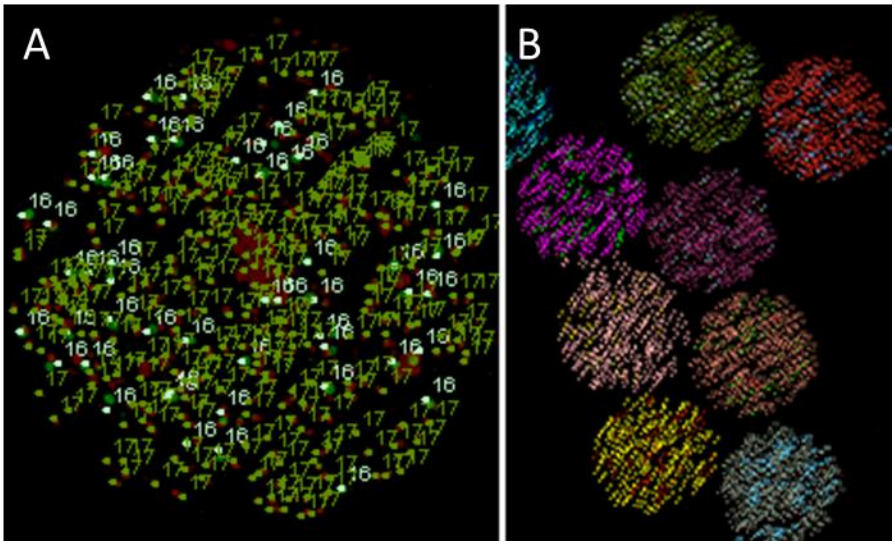

Figure 18. Cells of capsules manually counted with ImageJ. A) Cells of an individual capsules were numbered and colored corresponding to a group. B) Full tile scan image of a capsules which were counted manually.

Manual Cell Counting with ImageJ

ImageJ's Cell Counter plugin was used to manually count fluorescent cells. An observer enlarge a capsule to the size of screen and cells are marked and defined by manually selecting a group. Each mouse click marks a location with a colored square and number (Fig. 18). ImageJ tallies up each group and outputs the data in a table. Depending on the number of cells per capsule, the time of analysis can take from 1 minute to 10 minutes per capsule.

Semi-Automated Cell Counter:

The Semi-Automatic algorithm we developed first involves Manual Selection of Capsules followed by Automatic Cell Segmentation. The Manual mode has a region of interest tool with which the user crops a single capsule out of the image. The Automatic mode applies image processing algorithms to quantify the number of cells in the cropped images. The Automatic mode contains the following steps in order:

1) The red and green channels are separated and the resolution is increased.
2) The signal to noise ratio is increased.
3) The circumference of the cells is used to define the external watershed marker.
4) The cell centroid is used to define the internal watershed marker.
5) The watershed algorithm is implemented to segment the cells.
6) Segmentations are plotted on the original image for verification.

The manual and automatic modes are explained in more detail below.

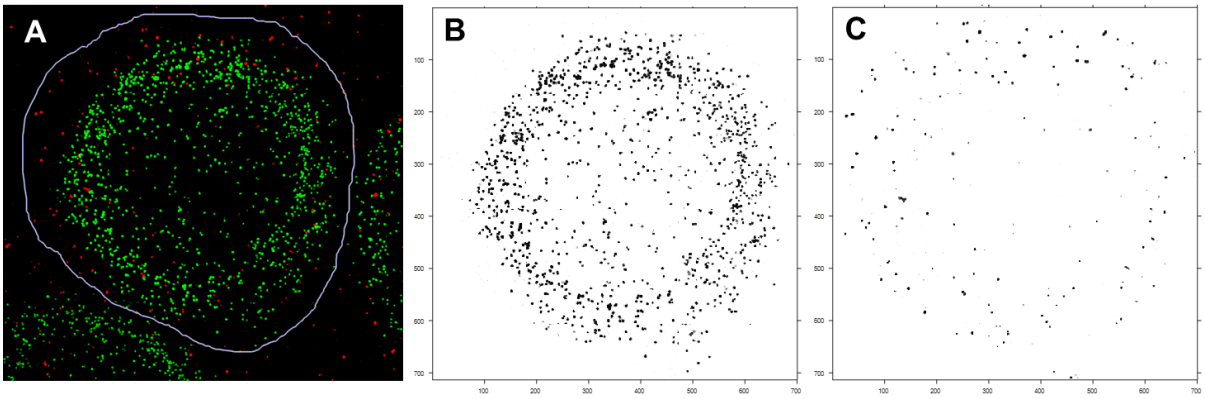

Fig. 19. A) Unmodified Live Dead Image was selected by outlining it in blue from which the green (B) and red (C) signals were extracted and counted separately.

Manual Selection of Capsules

In the Manual mode a region of interest tool is used to crops a single capsule out of the image containing multiple capsules. A region of interest is defined by manually outlining a depolymerized capsule within which the number of live and dead cells are

quantified by the algorithm. After the region of interest is selected, the image is cropped by the program and prepared for the automatic portion (Fig. 19A).

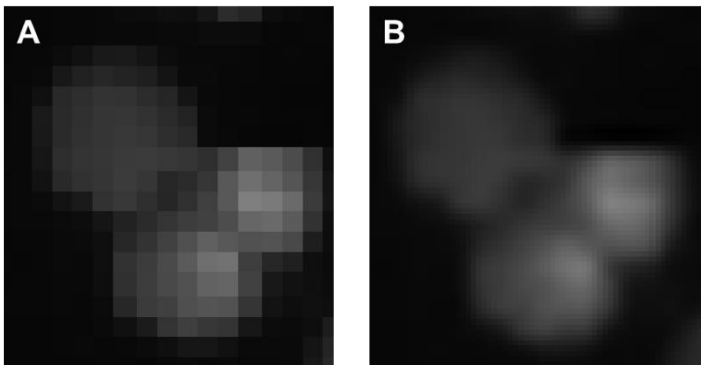

Figure 20: A) Original resolution of 3 cells. Each cells has a radius of 3 to 5 pixels. B) Bicubic Interpolation is used to increase the number of pixels representing a cell (B).

Automatic Cell Segmentation

Step 1 Channel Extraction and Image Resolution Increase: After a single capsule is extracted from the image through the manual portion, the green and red channels are separated (Fig. 19 B & C). The green and red channels represent live and dead cells, respectively. To increase resolution of the epifluorescent microscope, cells are represented by cirlces with a radius of 3 to 4 pixels (Fig. 20A). This is an inadequate number of pixels for image processing techniques. Therefore, the image size is increased, using a bicubic interpolation method. Bicubic interpolation calculates the value of a new data point by considering 16 known pixel values (Fig. 20B).

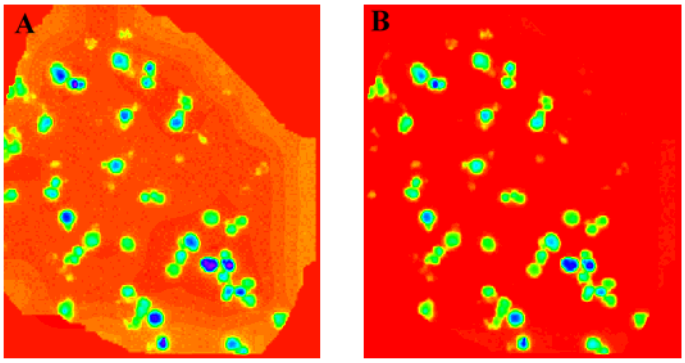

Figure 21. Green Channel. Color map of image is changed to show noise. A contrast limited adaptive histogram and 2-D Noise adaptive filter applied on Fig. 20A resulting in Fig. 20B.

Step 2 Increase Signal to Noise Ratio: A contrast limited adaptive histogram equalization was used to enhance the contrast in small regions in the image [54]. Thn a 2-D adaptive noise filter is applied to the image that removes constant power additive noise (e.g. Gaussian noise) [54]. These algorithms output a base image for image processing (Fig. 21B).

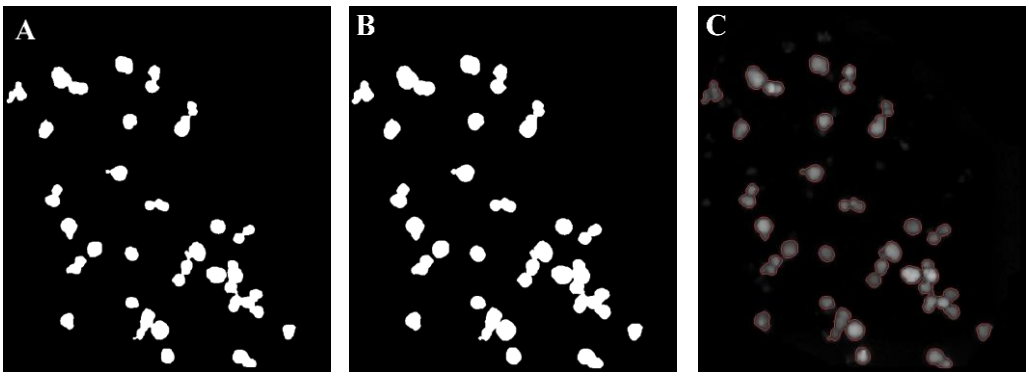

Figure 22. Green Channel. A): Otsu's Global Threshold is applied on Fig 21B. B): Morphological Operations are applied on Fig. 22A. C): The binary image is traced and plotted on top of the green live channel for validation.

Step 3 Define External Watershed Marker: In this step the external watershed marker was defined. Using Otsu's method, a global threshold is applied on the base images from

Step 2. Otsu's method assumes the image contains two classes of intensity pixels, and calculates the ideal threshold to separate them (Fig. 22A) [54]. To clean up the resulting thresholded image, post processing techniques are applied in the following order: Filling, Erosion, Dilation, and Size Threshold (Fig. 22B). The "Filling" algorithm fills in holes in the binary image. "Erosion" and "Dilation" respectively erode away and dilate the boundary regions. "Size Threshold" removes small objects from the binary image under a given threshold. After these morphological operations, the binary image is traced for validation (Fig. 22C) [54].

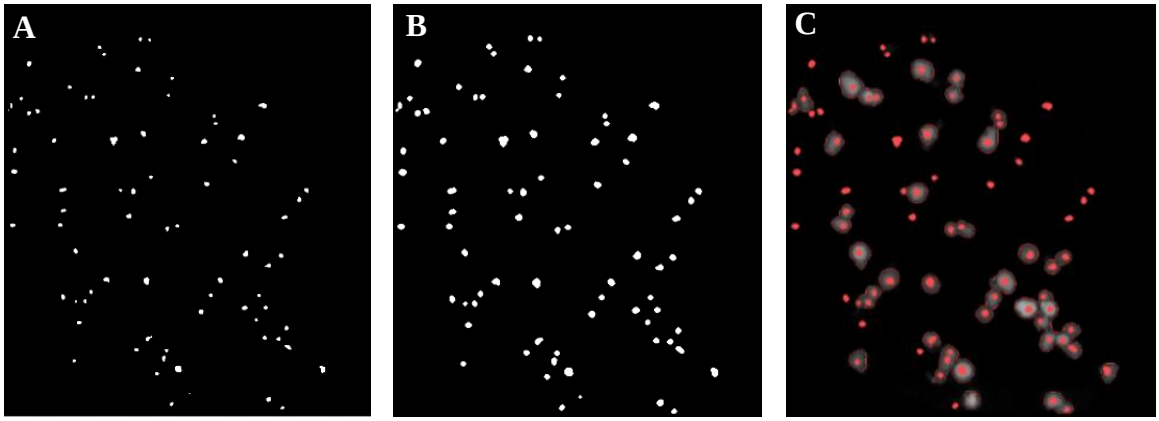

Figure 23. Green Channel. A): The regional maxima is performed on Fig. 22B. B): Morphological Operations are applied on Fig. 23A. C): Cell Centroids are overlaid on Fig. 22C.

Step 4 Define Internal Watershed Marker: The internal watershed marker for cell segmentation was chosen to represent the cell center. The H-maxima transform algorithm labels points in the image with intensity values over a given threshold. The location of the maximum intensity should be located in the centroid of the cell. To remove double positives, morphological operations were performed: Close, Fill, Erosion, Dilate, and Size Threshold (Fig. 23B). The morphological operation "Close" performs "Dilation"

only in the interior region of the binary image, preventing destruction of labeled cell centroid. Next “Erosion” and “Dilation” are performed to remove unwanted artifacts. Finally, “Size Threshold” is used to remove small objects from the image under a given threshold. For validation, these cell centroid points are plotted on top of the traced image (Fig. 23C).

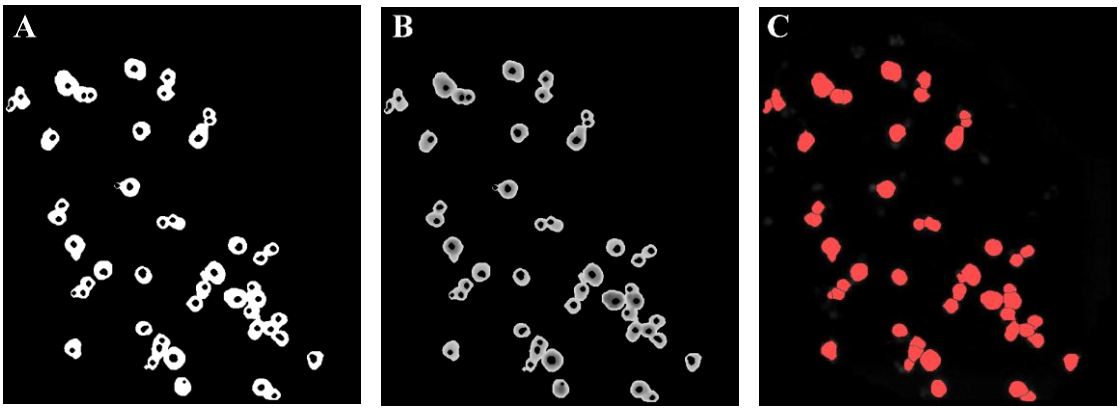

Figure 24. Green Channel. A): Cell centroids are removed from the threshold binary image. B): A regional minimum was used to create a decrease in intensity towards the cell centroid. C): Watershed was performed and overlaid on original green channel for validation.

Step 5 Watershed Algorithm: The watershed algorithm is able to divide groups of cells based on the intensity of a grayscale image. It treats the image as a topographic map, where high intensity pixels represent high elevations and dark pixels represent low elevations [54]. For the watershed algorithm to be most efficient, the cell borders need to have the highest intensity, and the background and centroids need to have the lowest intensity. This was done by subtracting the cell centroid image (Fig. 23B) against the threshold image (Fig. 22A). As seen in Fig. 24A, each cell center had a minimum point. Afterwards a regional minimum was imposed at the centroids of the cell, creating an intensity gradient towards the centroid (Fig. 24B). This allows watershed to segment the cells more accurately.

Step 6 Verification: At this stage, the watershed algorithm was applied on Fig. 24B and overlaid on the original image (Fig. 24C). The number of live and dead cells was output from the algorithm. To verify that the algorithm correctly detected and counted the number of live/dead cells, the automatic cell counter is compared to the manual human counter.

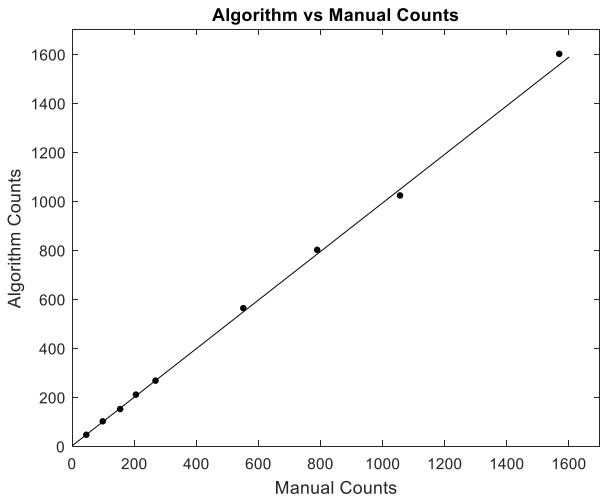

Figure 25. The semi-automated cell counter was compared to a human counter using ImageJ. f(x)=0.991x+1.632, R-squared: 0.999.

A.3 Results:

This semi-automated live and dead cell counter for depolymerized capsules is able to successfully identify and count individual cells. As shown in Fig. 25, the quality of the semi-automated counter was confirmed when compared to a manual human counter. Regardless of the density of cells per capsule, both the manual and semi-automated cell counter quantified a similar number of cells. The average counting time per capsule with about 1000 cells for the manual ImageJ is about 5 minutes. The average counting time per capsule for the semi-automated cell counter is about 10 seconds. Thus, the semi-automated cell counter approach is approximately 35 times faster.

A.4 Discussion:

The semi-automated counter developed is able to successfully identify and count cells in a more quantitative and objective method than Manual Cell Counting with ImageJ. Future optimizations with the morphological processing techniques can be done on the algorithm to increase the sensitivity and specificity. The over segmentation issue can be solved by introducing a merging algorithm which combines attached cells under a size threshold. This will decrease the false positives, thereby increasing the specificity of the algorithm. By using less harsh erosion operations, lower intensity cells will be preserved. This will decrease the false negatives, thus increasing the sensitivity of the algorithm. We have demonstrated that the semi-automated cell counter is reliable but routine use will require additional algorithms. The current algorithm does not remove large artifacts (e.g. dust) in the image. In the future, a size and shape exclusion tool will be developed to automatically remove large or elongated objects from the image (e.g. depolymerized alginate, dust).

We will calibrate this cell counter for cell types of different sizes such as: Mesenchymal Stem Cells, Chinese Hamster Ovarian Cells, and Hybridomas, which have diameters ranging from 5 μm to 20 μm for the non-adhered spherical cells.

The semi-automated counter is approximately 35 times faster than the manual cell counter and more objective. Manually counting over 10,000 cells in an hour is time consuming and labor-intensive. Over time, the manual counter's quality may deteriorate. In addition, we expect that different manual counters will have different classification for low intensity cells. Thus, manually counting data may be subjective while the semi-automated counter is totally objective, yielding more consistent and accurate data. In

summary, we developed a semi-automatic method to count number of live and dead cells in a region of interest using images acquired by epifluorescence microscopy.

REFERENCES

1. Uccelli, A., L. Moretta, and V. Pistoia, *Mesenchymal stem cells in health and disease.* Nat Rev Immunol, 2008. **8**(9): p. 726-36.
2. Selimoglu, S.M. and M. Elibol, *Alginate as an immobilization material for MAb production via encapsulated hybridoma cells.* Crit Rev Biotechnol, 2010. **30**(2): p. 145-59.
3. Sikorski, P., et al., *Evidence for Egg-Box-Compatible Interactions in Calcium−Alginate Gels from Fiber X-ray Diffraction.* Biomacromolecules, 2007. **8**(7): p. 2098-2103.
4. Mørch, Y., *Novel Alginate Microcapsules for Cell Therapy -A study of the structure-function relationships in native and structurally engineered alginates*. 2018.
5. Wu, X., R. Oleschuk, and N. Cann, *Characterization of microstructured fibre emitters: In pursuit of improved nano electrospray ionization performance*. Vol. 137. 2012. 4150-61.
6. Caplan, A.I. and J.E. Dennis, *Mesenchymal stem cells as trophic mediators.* J Cell Biochem, 2006. **98**(5): p. 1076-84.
7. Pistoia, V. and L. Raffaghello, *Mesenchymal stromal cells and autoimmunity.* Int Immunol, 2017. **29**(2): p. 49-58.
8. Ma, S., et al., *Immunobiology of mesenchymal stem cells.* Cell Death Differ, 2014. **21**(2): p. 216-25.
9. Kumar, S., et al., *Sizes and Sufficient Quantities of MSC Microspheres for Intrathecal Injection to Modulate Inflammation in Spinal Cord Injury.* Nano LIFE, 2015. **05**(04): p. 1550004.
10. Parekkadan, B., et al., *Bone marrow stromal cell transplants prevent experimental enterocolitis and require host CD11b+ splenocytes.* Gastroenterology, 2011. **140**(3): p. 966-75.
11. Yagi, H., et al., *Bone marrow mesenchymal stromal cells attenuate organ injury induced by LPS and burn.* Cell Transplant, 2010. **19**(6): p. 823-30.
12. Zhang, M., et al., *SDF-1 expression by mesenchymal stem cells results in trophic support of cardiac myocytes after myocardial infarction.* Faseb j, 2007. **21**(12): p. 3197-207.
13. van Poll, D., et al., *Mesenchymal stem cell-derived molecules directly modulate hepatocellular death and regeneration in vitro and in vivo.* Hepatology, 2008. **47**(5): p. 1634-43.
14. Parekkadan, B., A.W. Tilles, and M.L. Yarmush, *Bone marrow-derived mesenchymal stem cells ameliorate autoimmune enteropathy independently of regulatory T cells.* Stem Cells, 2008. **26**(7): p. 1913-9.
15. Polchert, D., et al., *IFN-gamma activation of mesenchymal stem cells for treatment and prevention of graft versus host disease.* Eur J Immunol, 2008. **38**(6): p. 1745-55.
16. Ohtaki, H., et al., *Stem/progenitor cells from bone marrow decrease neuronal death in global ischemia by modulation of inflammatory/immune responses.* Proc Natl Acad Sci U S A, 2008. **105**(38): p. 14638-43.

17. Barker, R.A. and H. Widner, *Immune problems in central nervous system cell therapy.* NeuroRx, 2004. **1**(4): p. 472-81.
18. Li, Z.H., et al., *Intravenous transplantation of allogeneic bone marrow mesenchymal stem cells and its directional migration to the necrotic femoral head.* Int J Med Sci, 2011. **8**(1): p. 74-83.
19. Bakshi, A., et al., *Minimally invasive delivery of stem cells for spinal cord injury: advantages of the lumbar puncture technique.* J Neurosurg Spine, 2004. **1**(3): p. 330-7.
20. Trouche, E., et al., *Evaluation of alginate microspheres for mesenchymal stem cell engraftment on solid organ.* Cell Transplant, 2010. **19**(12): p. 1623-33.
21. Paredes Juarez, G.A., et al., *Immunological and technical considerations in application of alginate-based microencapsulation systems.* Front Bioeng Biotechnol, 2014. **2**: p. 26.
22. Vegas, A.J., et al., *Long-term glycemic control using polymer-encapsulated human stem cell-derived beta cells in immune-competent mice.* Nat Med, 2016.
23. Gurruchaga, H., et al., *Advances in cell encapsulation technology and its application in drug delivery.* Expert Opin Drug Deliv, 2015. **12**(8): p. 1251-67.
24. Skaugrud, O., et al., *Biomedical and pharmaceutical applications of alginate and chitosan.* Biotechnol Genet Eng Rev, 1999. **16**: p. 23-40.
25. Lanza, R.P. and W.L. Chick, *Immunoisolation: at a turning point.* Immunol Today, 1997. **18**(3): p. 135-9.
26. Acarregui, A., et al., *A perspective on bioactive cell microencapsulation.* BioDrugs, 2012. **26**(5): p. 283-301.
27. Smidsrod, O., *Molecular basis for some physical properties of alginates in the gel state.* Faraday Discussions of the Chemical Society, 1974. **57**(0): p. 263-274.
28. Dentini, M., et al., *Comparative studies on solution characteristics of mannuronan epimerized by C-5 epimerases.* Carbohydrate Polymers, 2005. **59**(4): p. 489-499.
29. Stokke, B.T., O. Smidsrød, and D.A. Brant, *Predicted influence of monomer sequence distribution and acetylation on the extension of naturally occurring alginates.* Carbohydrate Polymers, 1993. **22**(1): p. 57-66.
30. Smidsrød, O., R.M. Glover, and S.G. Whittington, *The relative extension of alginates having different chemical composition.* Carbohydrate Research, 1973. **27**(1): p. 107-118.
31. Barminko, J., et al., *Encapsulated mesenchymal stromal cells for in vivo transplantation.* Biotechnol Bioeng, 2011. **108**(11): p. 2747-58.
32. Landazuri, N., et al., *Alginate microencapsulation of human mesenchymal stem cells as a strategy to enhance paracrine-mediated vascular recovery after hindlimb ischaemia.* J Tissue Eng Regen Med, 2016. **10**(3): p. 222-32.
33. Levit, R.D., et al., *Cellular encapsulation enhances cardiac repair.* J Am Heart Assoc, 2013. **2**(5): p. e000367.
34. Landazuri, N., et al., *Alginate microencapsulation of human mesenchymal stem cells as a strategy to enhance paracrine-mediated vascular recovery after hindlimb ischaemia.* J Tissue Eng Regen Med, 2012.

35. Grandoso, L., et al., *Long-term survival of encapsulated GDNF secreting cells implanted within the striatum of parkinsonized rats.* Int J Pharm, 2007. **343**(1-2): p. 69-78.
36. Klinge, P.M., et al., *Encapsulated native and glucagon-like peptide-1 transfected human mesenchymal stem cells in a transgenic mouse model of Alzheimer's disease.* Neurosci Lett, 2011. **497**(1): p. 6-10.
37. Tobias, C.A., et al., *Alginate encapsulated BDNF-producing fibroblast grafts permit recovery of function after spinal cord injury in the absence of immune suppression.* J Neurotrauma, 2005. **22**(1): p. 138-56.
38. Goren, A., et al., *Encapsulated human mesenchymal stem cells: a unique hypoimmunogenic platform for long-term cellular therapy.* FASEB J, 2010. **24**(1): p. 22-31.
39. Tiziana, S., P. Gianfranco, and G. Umberto, *Clinical Trials with Mesenchymal Stem Cells: An Update.* Cell Transplantation, 2016. **25**(5): p. 829-848.
40. Jacobs, S.A., et al., *Immunological characteristics of human mesenchymal stem cells and multipotent adult progenitor cells.* Immunol Cell Biol, 2013. **91**(1): p. 32-9.
41. Fischer, U.M., et al., *Pulmonary Passage is a Major Obstacle for Intravenous Stem Cell Delivery: The Pulmonary First-Pass Effect.* Stem Cells and Development, 2009. **18**(5): p. 683-691.
42. Orive, G., et al., *Application of cell encapsulation for controlled delivery of biological therapeutics.* Adv Drug Deliv Rev, 2014. **67-68**: p. 3-14.
43. Lee, S.-H., X.H. Nguyen, and H.S. Ko, *Study on droplet formation with surface tension for electrohydrodynamic inkjet nozzle.* Journal of Mechanical Science and Technology, 2012. **26**(5): p. 1403-1408.
44. Rahman, K., et al., *Simulation of droplet generation through electrostatic forces.* Journal of Mechanical Science and Technology, 2010. **24**(1): p. 307-310.
45. Nedović, V.A., et al., *Electrostatic generation of alginate microbeads loaded with brewing yeast.* Process Biochemistry, 2001. **37**(1): p. 17-22.
46. Davarcı, F., et al., *The influence of solution viscosities and surface tension on calcium-alginate microbead formation using dripping technique.* Food Hydrocolloids, 2017. **62**: p. 119-127.
47. Goosen, M., et al., *Electrostatic Droplet Generation for Encapsulat ion of Somatic Tissue: Assessment of High-Voltage Power Supply*. Vol. 13. 2008. 497-502.
48. Huang, H., et al., *Stiffness-Independent Highly Efficient On-Chip Extraction of Cell-Laden Hydrogel Microcapsules from Oil Emulsion into Aqueous Solution by Dielectrophoresis.* Small, 2015. **11**(40): p. 5369-5374.
49. Gryshkov, O., et al., *Process engineering of high voltage alginate encapsulation of mesenchymal stem cells.* Materials Science and Engineering: C, 2014. **36**: p. 77-83.
50. Leijs, M.J., et al., *Encapsulation of allogeneic mesenchymal stem cells in alginate extends local presence and therapeutic function.* Eur Cell Mater, 2017. **33**: p. 43-58.

51. Heile, A.M., et al., *Cerebral transplantation of encapsulated mesenchymal stem cells improves cellular pathology after experimental traumatic brain injury.* Neurosci Lett, 2009. **463**(3): p. 176-81.
52. ThermoFisher. *Counting Cells in a Hemacytometer*. 2018 14 March 2018]; Available from: https://www.thermofisher.com/us/en/home/references/gibco-cell-culture-basics/cell-culture-protocols/counting-cells-in-a-hemacytometer.html.
53. Yongming, C., et al. *An automatic cell counting method for optical images*. in *Proceedings of the First Joint BMES/EMBS Conference. 1999 IEEE Engineering in Medicine and Biology 21st Annual Conference and the 1999 Annual Fall Meeting of the Biomedical Engineering Society (Cat. N*. 1999.
54. Semmlow, J.L., *Biosignal and biomedical image processing : MATLAB-based applications*. 2004: New York : Marcel Dekker.